1521-009X/48/2/75–84$35.00
Drug Metabolism and Disposition

https://doi.org/10.1124/dmd.119.088229
Drug Metab Dispos 48:75–84, February 2020

Glucuronidation of Abiraterone and Its Pharmacologically Active Metabolites by UGT1A4, Influence of Polymorphic Variants and Their Potential as Inhibitors of Steroid Glucuronidation [S]

Joanie Vaillancourt, Véronique Turcotte, Patrick Caron, Lyne Villeneuve, Louis Lacombe, Frédéric Pouliot, Éric Lévesque, and Chantal Guillemette

Pharmacogenomics Laboratory, Centre Hospitalier Universitaire de Québec (CHU de Québec) Research Center – Université Laval and Faculty of Pharmacy (J.V., V.T., P.C., L.V., C.G.), CHU de Québec Research Center – Université Laval, Division of Urology, Faculty of Medicine, Surgery Department (L.L., F.P.), and CHU de Québec Research Center – Université Laval, Division of Hematology-Oncology, Faculty of Medicine (E.L.), Laval University, Québec, Canada

Received June 7, 2019; accepted November 8, 2019

ABSTRACT

Abiraterone (Abi) acetate (AA) is a prodrug of Abi, a CYP17A1 inhibitor used to treat patients with advanced prostate cancer. Abi is a selective steroidal inhibitor that blocks the biosynthesis of androgens. It undergoes extensive biotransformation by steroid pathways, leading to the formation of pharmacologically active Δ^4-Abi (D4A) and 5α-Abi. This study aimed to characterize the glucuronidation pathway of Abi and its two active metabolites. We show that Abi, its metabolites, and another steroidal inhibitor galeterone (Gal) undergo secondary metabolism to form glucuronides (G) in human liver microsomes with minor formation by intestine and kidney microsomal preparations. The potential clinical relevance of this pathway is supported by the detection by liquid chromatography–tandem mass spectrometry of Abi-G, D4A-G, and 5α-Abi-G in patients under AA therapy. A screening of UGT enzymes reveals that UGT1A4 is the main enzyme involved. This is supported by inhibition experiments using a selective UGT1A4 inhibitor hecogenin. A number of common and rare nonsynonymous variants significantly abrogate the UGT1A4-mediated formation of Abi-G, D4A-G, and 5α-Abi-G in vitro. We also identify Gal, Abi, and its metabolites as highly potent inhibitors of steroid inactivation by the UGT pathway with submicromolar inhibitor constant values. They reduce the glucuronidation of both the adrenal precursors and potent androgens in human liver, prostate cancer cells, and by recombinant UGTs involved in their inactivation. In conclusion, tested CYP17A1 inhibitors are metabolized through UGT1A4, and germline variations affecting this metabolic pathway may also influence drug metabolism.

SIGNIFICANCE STATEMENT

The antiandrogen abiraterone (Abi) is a selective steroidal inhibitor of the cytochrome P450 17α-hydroxy/17,20-lyase, an enzyme involved in the biosynthesis of androgens. Abi is metabolized to pharmacologically active metabolites by steroidogenic enzymes. We demonstrate that Abi and its metabolites are glucuronidated in the liver and that their glucuronide derivatives are detected at variable levels in circulation of treated prostate cancer patients. UDP-glucuronosyltransferase (UGT)1A4 is the primary enzyme involved, and nonsynonymous germline variations affect this metabolic pathway in vitro, suggesting a potential influence of drug metabolism and action in patients. Their inhibitory effect on drug and steroid glucuronidation raises the possibility that these pharmacological compounds might affect the UGT-associated drug-metabolizing system and pre-receptor control of androgen metabolism in patients.

Introduction

Prostate cancer (PCa) is the leading cause of cancer in men and the second cause of death in Western countries (Miller et al., 2016). Much progress has been made in the last few years with new generation hormonal therapies. Abiraterone (Abi) and enzalutamide have significantly changed clinical management, increasing survival and quality of life of patients with metastatic PCa (Fizazi et al., 2012; Scher et al., 2012; Beer et al., 2014; Ryan et al., 2015; Tucci et al., 2015). In advanced disease, PCa cells remain dependent on androgens for proliferation (Montgomery et al., 2008). Therefore, Abi, orally administered as the prodrug Abi acetate (AA), is commonly used as part of the androgen deprivation therapy in advanced disease clinical settings.

Part of this work was supported by the CHU de Québec – Université Laval Foundation, Québec, Canada (to E.L. and C.G.) and the Canada Research Chair Program (Grant 950-203962 to C.G.). E.L. holds a Canadian Institutes of Health Research (CIHR) Clinician-Scientist Award. C.G. holds the Canada Research Chair in Pharmacogenomics (Tier I). J.V. holds a Fonds de Recherche du Québec – Santé Studentship Award.

No conflict of interests was disclosed.

https://doi.org/10.1124/dmd.119.088229.

[S] This article has supplemental material available at dmd.aspetjournals.org.

ABBREVIATIONS: A5-diol, androstanediol; AA, Abi acetate; Abi, abiraterone; CYP17A1, cytochrome P450 17α-hydroxy/17,20-lyase; D4A, Δ^4-Abi; DHEA, dehydroepiandrosterone; DHT, dihydrotestosterone; G, glucuronide; Gal, galeterone; GlcA, glucuronic acid; HEK, human embryonic kidney; HLM, human liver microsome; K_i, inhibitor constant; K_m, Michaelis constant; LC, liquid chromatography; PCa, prostate cancer; Testo, testosterone; UGT, UDP-glucuronosyltransferase.

Abi is a selective steroidal inhibitor of the cytochrome P450 17α-hydroxy/17,20-lyase (CYP17A1), an enzyme involved in the biosynthesis of androgens. Abi is an androgen receptor axis–targeted agent that blocks the formation of androgens in testes, adrenal, peripheral tissues, and prostate tumor cells. Recently, new metabolites of Abi formed by steroidogenic enzymes have been described, with at least two exhibiting significant pharmacological activities, Δ^4-Abi (D4A) and 5α-Abi (Li et al., 2016). Abi is first converted to D4A by 3β-hydroxysteroid dehydrogenase and blocks CYP17A1, 3β-hydroxysteroid dehydrogenase, and steroid-5α-reductase, whereas D4A also antagonizes the androgen receptor (Li et al., 2015). D4A is irreversibly converted to 3-keto-5α-Abi or 3-keto-5β-Abi. Both metabolites may then be converted to their 3α-OH and 3β-OH derivatives for a total of six downstream metabolites of D4A. The 5β-Abi metabolites were not reported to be active. In contrast, the direct product of D4A, 5α-Abi, acts as an agonist of the androgen receptor (Li et al., 2016). Likewise, the structurally related CYP17A1 inhibitor galeterone (Gal) yields analogous metabolites (Alyamani et al., 2017).

We hypothesized that, similar to endogenous steroids, Abi, its metabolites, and the structurally related Gal (Supplemental Fig. 1) undergo direct metabolism by the glucuronidation pathway. A large family of 19 UDP-glucuronosyltransferase (UGT) enzymes catalyzes this phase II drug metabolic pathway (Guillemette et al., 2014). UGTs are involved in the addition of a glucuronic acid (GlcA) moiety to a large diversity of acceptor molecules, including therapeutic drugs from all classes containing hydroxyl, carboxylic acid, thiol, or amine groups (Guillemette et al., 2014). This leads to the formation of glucuronide (G) derivatives that most often lack biologic activity and that are readily excreted through bile and urine. This pathway also catalyzes the clearance of steroids such as the potent androgen dihydrotestosterone (DHT) and thereby regulates their bioavailability and the hormonal environment to which PCa cells are exposed (Beaulieu et al., 1996). The UGT pathway undergoes complex regulation. This involves regulatory loops characterized by the ability of UGT substrates to regulate the expression of genes encoding UGT enzymes involved in their metabolism (Hu et al., 2014). We further postulated that CYP17A1 inhibitors potentially influence endogenous steroid metabolism by affecting their conjugation by UGTs.

In this study, we report that Abi and its metabolites as well as Gal undergo metabolism by the UGT pathway and that they inhibit inactivation of steroids. Results of these in vitro investigations are reinforced by the detection of G derivatives of Abi, D4A, and 5α-Abi in PCa patients treated with AA.

Materials and Methods

Chemicals and Reagents. All chemicals and reagents were of the highest grade commercially available. UDP-GlcA and bilirubin were obtained from Sigma-Aldrich (Oakville, ON, Canada). All chemicals and solvents used for the mass spectrometry were high-pressure liquid chromatography (LC) grade. Milli-Q water was produced using the Millipore system. Abi and Gal were purchased from Toronto Research Chemical (Toronto, ON, Canada). Tacrolimus (FK-506) was purchased from Cell Signaling Technology (Danvers, MA). β-glucuronidase type VII from *Escherichia coli* was purchased from Sigma-Aldrich (St. Louis, MO). Hecogenin was obtained from Santa Cruz Biotechnology (Dallas, TX). The Organic Synthesis Service of the CHU de Québec Research Center (Quebec, QC, Canada) synthesized D4A and 5α-Abi based on a published method (Li et al., 2016). To identify D4A and 5α-Abi synthesized by the Medical Chemistry platform, NMR spectra were recorded on a Bruker Advance 400 digital spectrometer (Billerica, MA) at 400 MHz for ^{1}H NMR. Spectra were referenced relative to the central residual proton solvent resonance in ^{1}H NMR (CDCl3 = 7.26 ppm, MeOH-d4 = 3.31 ppm). High-pressure LC analyses for chemical purities (D4A 96% purity and 5α-Abi 98% purity) were performed on a Shimadzu Prominence instrument (Kyoto, Japan) using a diode array detector (wavelength detection = 190). Abi-G, D4A-G, 5α-Abi-G, and Gal-G analytical standards were produced from in vitro enzymatic assays, as described (Caron et al., 2019). Briefly, the G formed was treated with β-glucuronidase type VII from *E. coli* (50 U) incubated at 37°C for 20 hours in phosphate buffer (pH 6.5) to cleave the GlcA group and allow quantification with a calibration curve of the corresponding aglycone. Deuterated Gs were also produced and purified according to the same procedure. Microsomal preparations from human tissues [liver mixed gender pool of 50 individuals: cat. no. H0620, lot 1410013 (24 females, 26 males); 1210267 (19 females, 31 males) and 1610016 (20 females, 30 males); kidney mixed gender pool of eight individuals, cat. no. H0610.R, lot 0810236 (four females, four males); and colon mixed gender pool of seven, cat. no 452210, lot 05886 (four females, three males)] and commercial Supersomes [UGT1A1 (cat. no. 456411, lot 6320009), 1A3 (cat. no. 456413, lot 7065003), 1A4 (cat. no. 456414, lot 6334004, 7179004, and 8073001), 1A6 (cat. no. 456416, lot 6216001), 1A7 (cat. no. 456407, lot 4308001), 1A8 (cat. no. 456418, lot 7177002), 1A9 (cat. no. 456419, lot 7065002), 2B4 (cat. no. 456424, lot 6244003), 2B7 (cat. no. 456427, lot 7101003), 2B15 (cat. no. 456435, lot 5348003), and 2B17 (cat. no. 456437, lot 6312001, 8038005, and 8177003)] were purchased from Xenotech (Kansas City, KS), BD Biosciences (Woburn, MA), and Corning (Corning, NY), respectively. Microsomal protein extracts from human embryonic kidney (HEK)293-UGT1A4 cells expressing variant enzymes as well as LNCaP microsomes were prepared by differential centrifugation and quantified by Western blot, as described (Villeneuve et al., 2003; Laverdière et al., 2011).

Glucuronidation Assays. Enzymatic assays were conducted with 10 μg UGT membrane protein, 50 mM Tris-HCl (pH 7.5), 10 mM $MgCl_2$, 2 mM UDP-GlcA, pepstatin, leupeptin, and 20 μg/ml alamethicin in a final volume of 100 μl. The reactions were terminated by adding 100 μl methanol and were centrifuged at 14,000*g* for 10 minutes before analysis. Kinetics were conducted with microsomal fractions of a pool of 50 human livers, commercial UGT1A4 supersomes, and HEK293 recombinant human UGT1A4*1 ($R^{11}P^{24}L^{48}$), UGT1A4*2 (T^{24}), UGT1A4*3 (V^{48}), and UGT1A4*4 (W^{11}). Kinetics was performed using substrate concentrations ranging from 0.1 to 400 μM for 30 minutes. Additional assays were done with 2 μM AA and human liver microsomes (HLM) with an incubation time of 30 minutes and an overnight incubation to compare with Abi. Inhibition assays were performed using concentrations (0.5, 1, 2.5, 5, 10 μM) of a selective UGT1A4 inhibitor hecogenin and a constant concentration near Michaelis constant (K_m) of substrates for 30 minutes. The IC_{50} was then calculated using GraphPad (7.0; GraphPad Software, La Jolla, CA). The inhibitor constant (K_i) values were evaluated using concentrations of hecogenin (0.5, 1, 2.5, 5, 10 μM) and three different concentrations of each substrate (Abi: 2, 100, 200 μM; D4A: 6, 100, 200 μM; 5α-Abi: 5, 100, 200 μM; Gal: 0.5, 2, 5 μM). The inhibition of steroid glucuronidation was performed using Abi, D4A, 5α-Abi, and Gal as inhibitors and by monitoring glucuronidation of two potent androgens [testosterone (Testo), DHT] and their adrenal precursors [dehydroepiandrosterone (DHEA) and androstanediol (A5-diol)]. Those assays were performed for 30 minutes using three concentrations of inhibitors (5, 25, 200 μM) and three concentrations of substrates (5, 25, 200 μM), as indicated in the legends of figures.

Kinetics parameters were determined by nonlinear regression using Sigma Plot 11.0 assisted by Enzyme Kinetics 1.3 (SSI, San Jose, CA) using the Marquardt–Levenberg algorithm, which solves nonlinear least square equations. The best-fitting enzyme kinetics models were subsequently determined using goodness-of-fit criteria, including the coefficient of determination (r^2 values), Akaike information criteria, S.E., and 95% confidence intervals, followed by a visual inspection of fitted functions. The enzyme kinetics was subsequently represented by Eadie–Hofstee plots for glucuronidation profiles or Lineweaver–Burk plots for inhibition models. Values are expressed as mean ± S.D. of triplicate determinations of at least two independent experiments. Enzymatic activities were considered statistically significant for P values <0.05, according to Student's t test variance analysis.

Prostate Cancer Patients Treated with AA. A study ongoing at our center recruits PCa patients treated with AA at 1000 mg daily dose (2018-4125; CHU de Québec). The study is conducted in accordance with the declaration of Helsinki, and all patients provided consent for this project. Plasma samples were collected at least 1 month after treatment initiation to assess steady state levels of Abi and its metabolites using a protocol described previously (Caron et al., 2019).

Mass Spectrometry Analyses. Detection of analytes was performed by high-performance LC coupled to a Q-TRAP mass spectrometer (API6500 mass

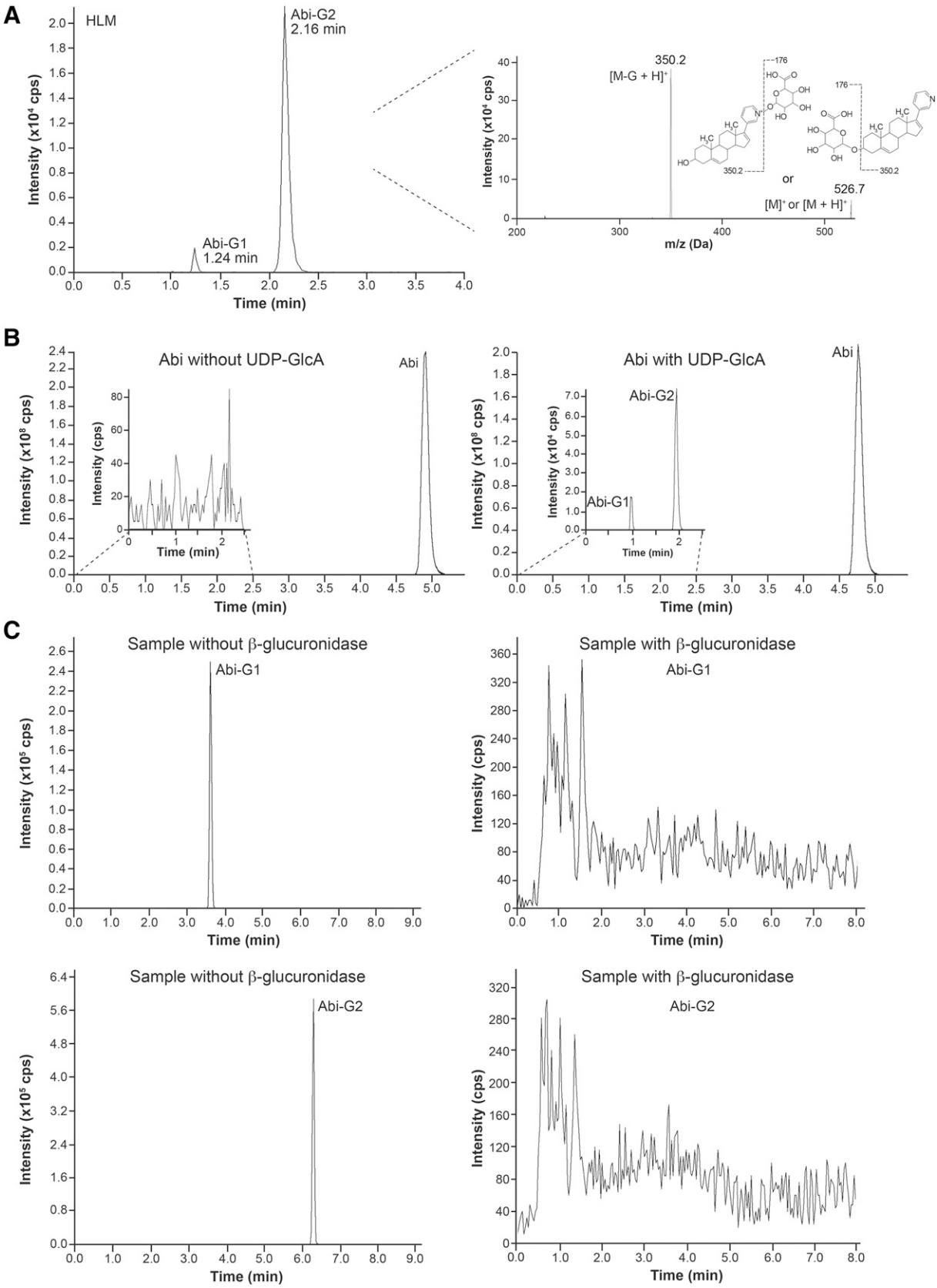

Fig. 1. Identification of two G metabolites of Abi. (A) Left: Chromatogram of the two polar metabolites observed after a 30-minute incubation of Abi with HLM at the transition 526.7 Da→350.2 Da. Metabolites were named G1 and G2 based on the order of elution. Right: The tandem mass spectrometry (MS/MS) fragmentation profile of the Gs. Masses of the protonated parent ion Abi-G $[M+H]^+$ or $[M]^+$ and of the fragment ion Abi $[M-G+H]^+$ are consistent with the loss of the G moiety (represented by the dashed line in each Abi-G structure). (B) These metabolites are observed in assays with HLM in the presence of the UGT cosubstrate, UDP-GlcA. (C) Polar metabolites disappear when incubated for 20 hours in presence of β-glucuronidase type VII from *Escherichia coli*.

TABLE 1

Detection of Abi, D4A, and 5α-Abi and their glucuronide derivatives in five prostate cancer patients under AA treatment

Patients	Steady State Blood Levels[a]													
	Abi		D4A		5α-Abi		Abi-G1		Abi-G2		D4A-G		5α-Abi-G	
	ng/ml	nM	ng/ml	nM	ng/ml	nM	ng/ml	nM	ng/ml	nM	ng/ml	nM	ng/ml	nM
AA-009	6.71	19.23	0.33	0.95	1.07	3.07	0.41	0.78	0.26	0.49	0.04	0.08	0.06	0.11
AA-015	35.10	100.57	1.92	5.53	10.00	28.65	0.81	1.54	1.39	2.64	0.18	0.34	0.60	1.14
AA-024	15.90	45.56	1.11	3.20	6.29	18.02	0.47	0.89	0.94	1.79	0.10	0.19	0.46	0.87
AA-025	62.60	179.37	3.53	10.17	8.88	25.44	0.34	0.65	1.28	2.43	0.02	0.04	0.20	0.38
AA-026	58.80	168.48	4.93	14.21	4.66	13.35	1.12	2.13	1.23	2.34	0.10	0.19	0.37	0.70
Mean	35.82	102.64	2.36	6.81	6.18	17.71	0.63	1.20	1.02	1.94	0.09	0.17	0.34	0.64
S.D.	24.95	71.49	1.86	5.36	3.55	10.16	0.33	0.62	0.46	0.87	0.06	0.12	0.21	0.40
CV	70%		79%		57%		52%		45%		69%		62%	

[a]Plasmatic concentrations correspond to C_{min} values and are similar to those observed in a previous group of five patients recruited at the same hospital (Caron et al., 2019).

spectrometer; AB Sciex, Concord, ON, Canada) using a validated method, as described (Caron et al., 2019). Briefly, the LC system consisted of a Nexera 30-AD (Shimadzu Scientific Instruments, Columbia, MD) controlled through Analyst Software, version 1.6.2. The mass spectrometer was operated in multiple reactions monitoring mode and equipped with a turbo spray source set at 500°C. The resolution used for Q1 and Q3 was Unit/Unit, and the voltage was held at 5500 V in positive mode. Mass transitions, ionization mode, declustering potential, collision energy, and lower limit of quantification were reported in Caron et al. (2019). For Gal, the chromatographic separation was identical as for Abi, whereas the multiple reactions monitoring mode transition for Gal-G1 and Gal-G2 was 565.2→389.2. The detection of tacrolimus-G and bilirubin-G was performed, as described (Lévesque et al., 2007; Laverdière et al., 2011). For the detection of DHT-G, Testo-G, DHEA-G, A5-diol-3G, and A5-diol-17G, the chromatographic separation was achieved with an ACE 3 C18 HL 3.0 μm packing material, 100 × 4.6 mm (Canadian Life Science, Peterborough, ON, Canada). The mobile phases were water, 1 mM ammonium formate (solvent A) and methanol, 1 mM ammonium formate (solvent B) at a flow rate of 0.9 ml/min. DHT-G (484.4→273.2) and DHEA-G (482.3→271.3) were detected in positive mode and eluted with 75% solvent B. Testo-G (463.1→75) was detected in negative mode and eluted with 75% solvent B. A5-diol-3G and A5-diol-17G (484.4→273.2) were detected in positive mode and eluted with the following gradient: 0 to 4.3 minutes, isocratic 50% B; 4.3 to 4.4 minutes, linear gradient 50% to 90% B; 4.4 to 5.4 minutes, isocratic 90% B; 5.4 to 5.5 minutes, 90% to 50% B; 5.5 to 8.0 minutes, isocratic 50% B.

Results

Glucuronidation of Abi, D4A, 5α-Abi, and Gal in Human Liver Microsomes and Their Detection in PCa Patients Treated with Abi. Enzymatic assays using pooled HLM revealed the formation of secondary polar metabolites of Abi, D4A, and 5α-Abi. One G derivative was observed upon D4A and 5α-Abi incubations, and two Gs were observed from Abi, named G1 and G2 according to the order of elution (Fig. 1A). The absence of polar metabolites in assays conducted without UDP-GlcA and their hydrolysis by β-glucuronidase treatment further supported that these metabolites correspond to G derivatives (Fig. 1, B and C). In vitro incubations in the same conditions, with the prodrug AA, generated similar results compared with Abi with no difference in the nature of the peaks formed and their abundance in HLM, likely due to its rapid conversion to Abi (Bouhajib and Tayab, 2019). Based on the presence of possible reactive groups, one possibly corresponds to a N-linked G of Abi (G1), whereas the other to an O-linked G (G2).

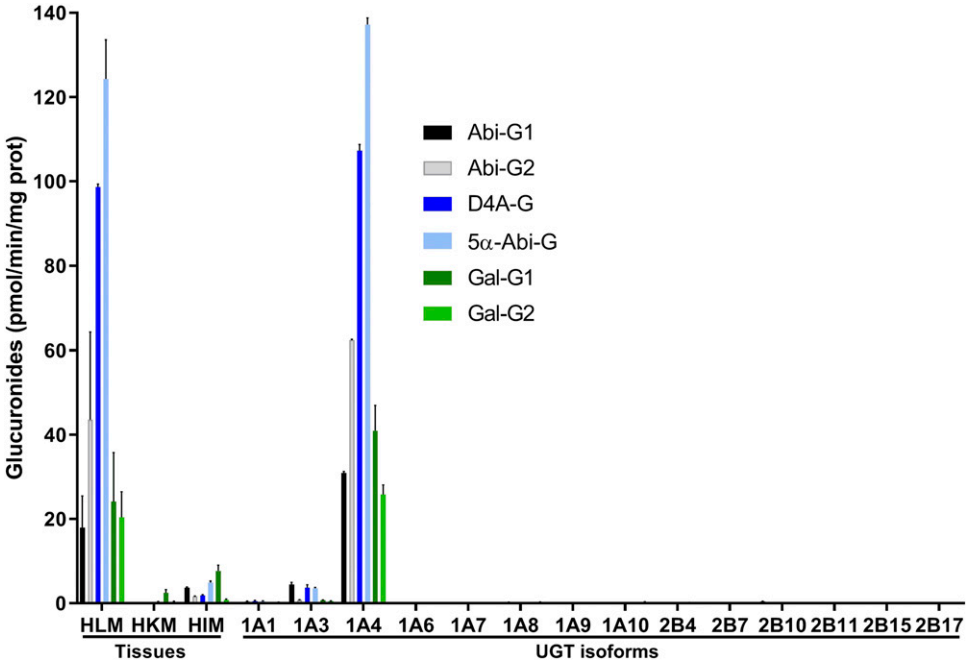

Fig. 2. Abi, D4A, 5α-Abi, and Gal glucuronidation by human tissues and recombinant human UGT enzymes. Glucuronidation activity of human tissues and recombinant UGTs (commercial supersomes and microsomes isolated from HEK293 cells for UGT1A10, UGT2B10, and UGT2B11) was measured at 200 μM substrate concentration for 2 hours. Results are expressed in picomoles per minute per milligram protein and as mean ± S.D. of duplicate determinations. The expression of individual UGT was confirmed by Western blotting, and the relative UGT expression between UGT1A3 and UGT1A4 supersomes was comparable, consistent with one of our previous reports using these protein preparations (Benoit-Biancamano et al., 2009b). HIM, human intestine microsomes; HKM, human kidney microsomes.

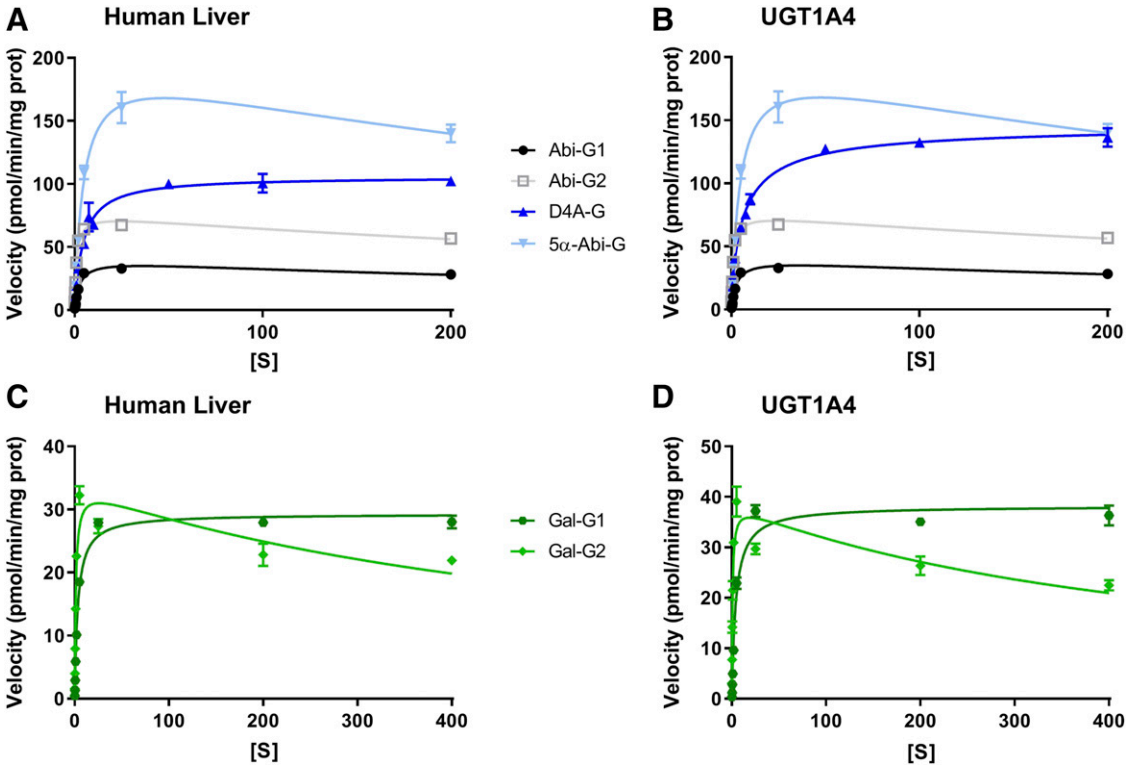

Fig. 3. Kinetic profiles for the formation of Gs of Abi, D4A, 5α-Abi, and Gal by HLM and recombinant UGT1A4 enzyme. (A, C) HLM and (B, D) UGT1A4 were incubated with concentrations ranging from 0 to 400 μM (A, B) Abi, D4A, 5α-Abi, or (C, D) Gal for 30 minutes, as described in *Materials and Methods*. Results are expressed as mean ± S.D. of triplicate determinations of one representative experiment.

This is supported by our previous analysis (Caron et al., 2019), in which we observed a loss of signal for Abi-G1 peak when analyzed in negative mode, whereas the signal for Abi-G2 remained. The loss of Abi-G1 peak is coherent with the quaternary amine being positively charged. Similarly, two Gs, G1 and G2, were observed for the structurally related CYP17A1 inhibitor Gal. A NMR-based analysis is required to clarify the identity of all G derivatives observed for Abi, D4A, 5α-Abi, and Gal.

A subset of PCa patients under AA therapy was analyzed to establish the presence of G derivatives of Abi and its metabolites in vivo, using a validated LC–tandem mass spectrometry method recently published by our group (Caron et al., 2019). Abi-G, D4A-G, and 5α-Abi-G were detected in circulation of patients at variable concentrations. Abi-G and 5α-Abi-G were measured in all patients, whereas D4A-G was below the lower limit of quantification (>5 ng/ml) for two patients (Table 1). A

TABLE 2

Enzyme kinetics of Abi, D4A, 5α-Abi, and Gal glucuronidation by human liver and the UGT1A4 enzyme

	Apparent K_m[a] (μM)	K_i (μM)	*N*	V_{max} (pmol/min/mg protein)	Clearance (μl/min/mg protein)
			Abiraterone		
			Abi-G1		
HLM	2.86 ± 0.25	446 ± 34		40.96 ± 1.12	14.38 ± 0.85
UGT1A4	2.80 ± 0.14	645 ± 3		43.47 ± 6.54	15.51 ± 1.55
			Abi-G2		
HLM	1.10 ± 0.12	551 ± 24		74.17 ± 3.00	67.89 ± 10.25
UGT1A4	0.72 ± 0.10	730 ± 216		66.75 ± 11.84	92.96 ± 3.53
			D4A-G		
HLM	4.52 ± 0.09	0.93 ± 0.10		125.02 ± 27.18	27.62 ± 5.49
UGT1A4	7.40 ± 1.36	0.81 ± 0.01		138.65 ± 11.99	19.21 ± 5.15
			5α-Abi-G		
HLM	5.07 ± 0.58	446 ± 52		206.19 ± 7.28	40.79 ± 3.24
UGT1A4	3.92 ± 0.02	1712 ± 430		222.83 ± 5.87	56.82 ± 1.84
			Galeterone		
			Gal-G1		
HLM	3.52 ± 0.84	1755 ± 850		33.59 ± 1.90	9.89 ± 2.90
UGT1A4	4.84 ± 1.20	1741 ± 398		40.08 ± 6.22	8.39 ± 0.79
			Gal-G2		
HLM	1.03 ± 0.25	538 ± 42		34.41 ± 0.80	34.50 ± 9.10
UGT1A4	0.61 ± 0.19	419 ± 75		34.90 ± 5.44	58.14 ± 8.80

[a]Results are expressed as mean ± S.D. of triplicate determinations of at least two independent experiments. Kinetic profiles observed were substrate inhibition for Abi-G1, Abi-G2, 5α-Abi-G, Gal-G1 and Gal-G2, and Hill for D4A-G.

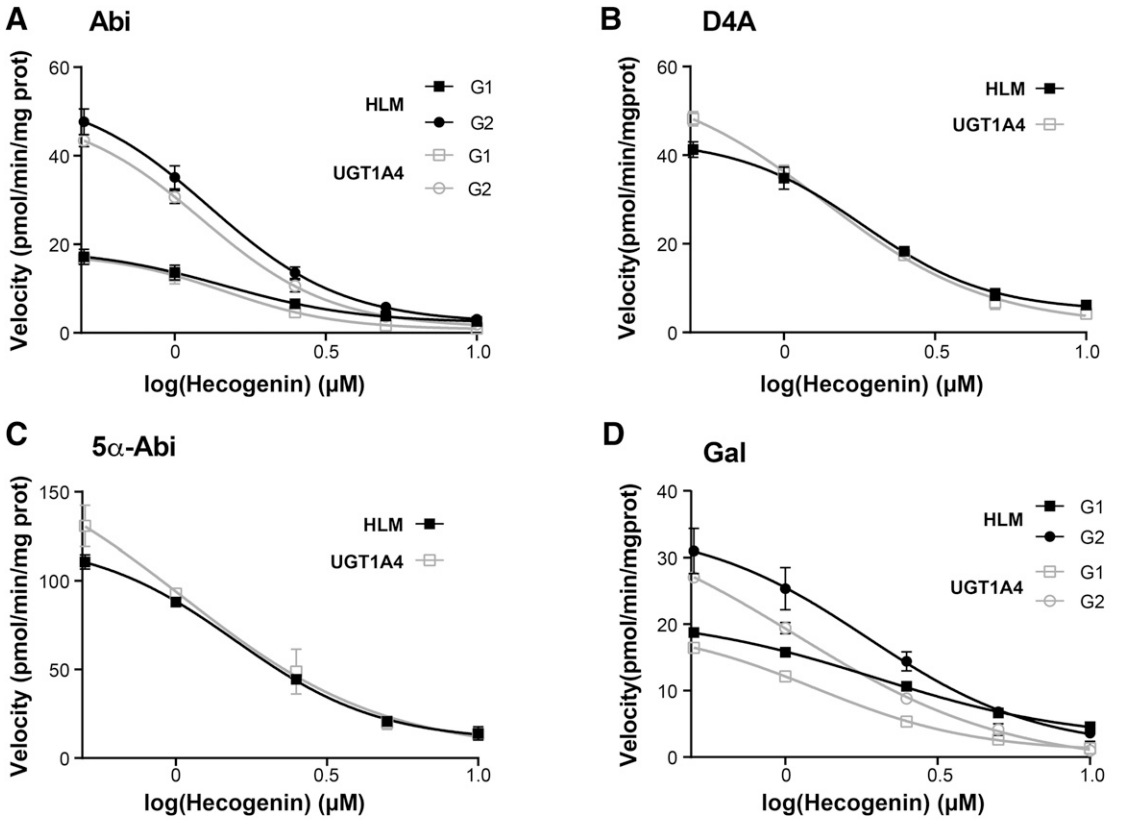

E

K_i (μM)	Abi		D4A	5α-Abi	Gal	
	G1	G2	G	G	G1	G2
HLM	0.66 ± 0.10	0.12 ± 0.02	0.62 ± 0.18	0.52 ± 0.34	1.05 ± 0.04	0.63 ± 0.13
UGT1A4	0.36 ± 0.00	0.10 ± 0.04	0.44 ± 0.33	0.29 ± 0.06	0.81 ± 0.05	0.48 ± 0.25

Fig. 4. Dose-dependent inhibition of Abi-G1, Abi-G2, D4A-G, 5α-Abi-G, Gal-G1, and Gal-G2 formation by hecogenin in HLM and recombinant UGT1A4 enzyme. (A–D) Inhibition profiles of Abi (A), D4A (B), 5α-Abi (C), and Gal (D) glucuronidation by hecogenin. Activity was measured at constant concentration of substrate (2 μM Abi, 6 μM D4A, 5 μM 5α-Abi, or 0.5 μM Gal) with six concentrations of hecogenin ranging from 0 to 10 μM for 30 minutes, as described in *Materials and Methods*. In the control, no hecogenin was added. (E) K_i values of Abi, D4A, 5α-Abi, and Gal by hecogenin measured using three different concentrations of substrate ranging from 2 to 200 μM with six concentrations of hecogenin ranging from 0 to 10 μM for 30 minutes, as described in *Materials and Methods*. Results are expressed as mean ± S.D. of triplicate determinations of at least two experiments. Inhibition models observed were mixed.

larger study is required to help clarify the clinical significance of this pathway.

UGT1A4-Mediated Glucuronidation of Abi and Its Metabolites: Kinetics Characterization and UGT1A4 Variants with Impaired Activity. Using recombinant human UGT enzymes, the hepatic UGT1A4 exhibited the highest glucuronidation activity for all four substrates, whereas UGT1A3 displayed much lower activity (Fig. 2). Screening experiments using 2 or 200 μM substrate for 2- or 16-hour incubations with any UGT did not result in the formation of Gs besides with UGT1A4 and at a much lower extent with UGT1A3 (data not shown). This is coherent with the expression profile of these two enzymes (Ohno and Nakajin, 2009; Margaillan et al., 2015), and the minor formation of G derivatives in the intestine and none detected in the kidney. Consistent with a major contribution of the UGT1A4 enzyme, kinetic parameters (apparent K_m, V_{max}, and clearance values) of all four substrates were almost identical for HLM and UGT1A4 (Fig. 3; Table 2). Eadie–Hofstee plots of HLM and recombinant UGT1A4 for all substrates are depicted in Supplemental Figs. 2–4 and suggest atypical and complex kinetics. Inhibition experiments with the selective UGT1A4 inhibitor hecogenin also led to highly comparable inhibition profiles and apparent K_i values (0.29–1.05 μM) between HLM and UGT1A4 for all four substrates, further supporting its major involvement (Fig. 4; Supplemental Fig. 7). Based on these results, we conclude that UGT1A4 is likely the only enzyme involved in the hepatic glucuronidation of Abi, D4A, 5α-Abi, and Gal. We also observed that these compounds were effective at inhibiting their glucuronidation, leading to similar levels of inhibition by ~30% to 50% in assays performed at K_m values in the liver and with the UGT1A4 enzyme (Supplemental Fig. 5). As an example, 2 μM Abi proficiently inhibited the formation of D4A-G by 29% and 41% in HLM and UGT1A4 recombinant system, respectively.

The impact of common *UGT1A4* coding region variations was then evaluated using recombinant UGT1A4 isoenzymes expressed in HEK293 human cells, namely UGT1A4*1 ($R^{11}P^{24}L^{48}$), UGT1A4*2 (T^{24}), UGT1A4*3 (V^{48}), and UGT1A4*4 (W^{11}) (Fig. 5). Compared with the UGT1A4*1 reference enzyme, the UGT1A4*4 isoenzyme presented a velocity reduced by nearly 50% for the conjugation of Abi, D4A, and 5α-Abi (Fig. 5D; Supplemental Table 1). UGT1A4*2 and

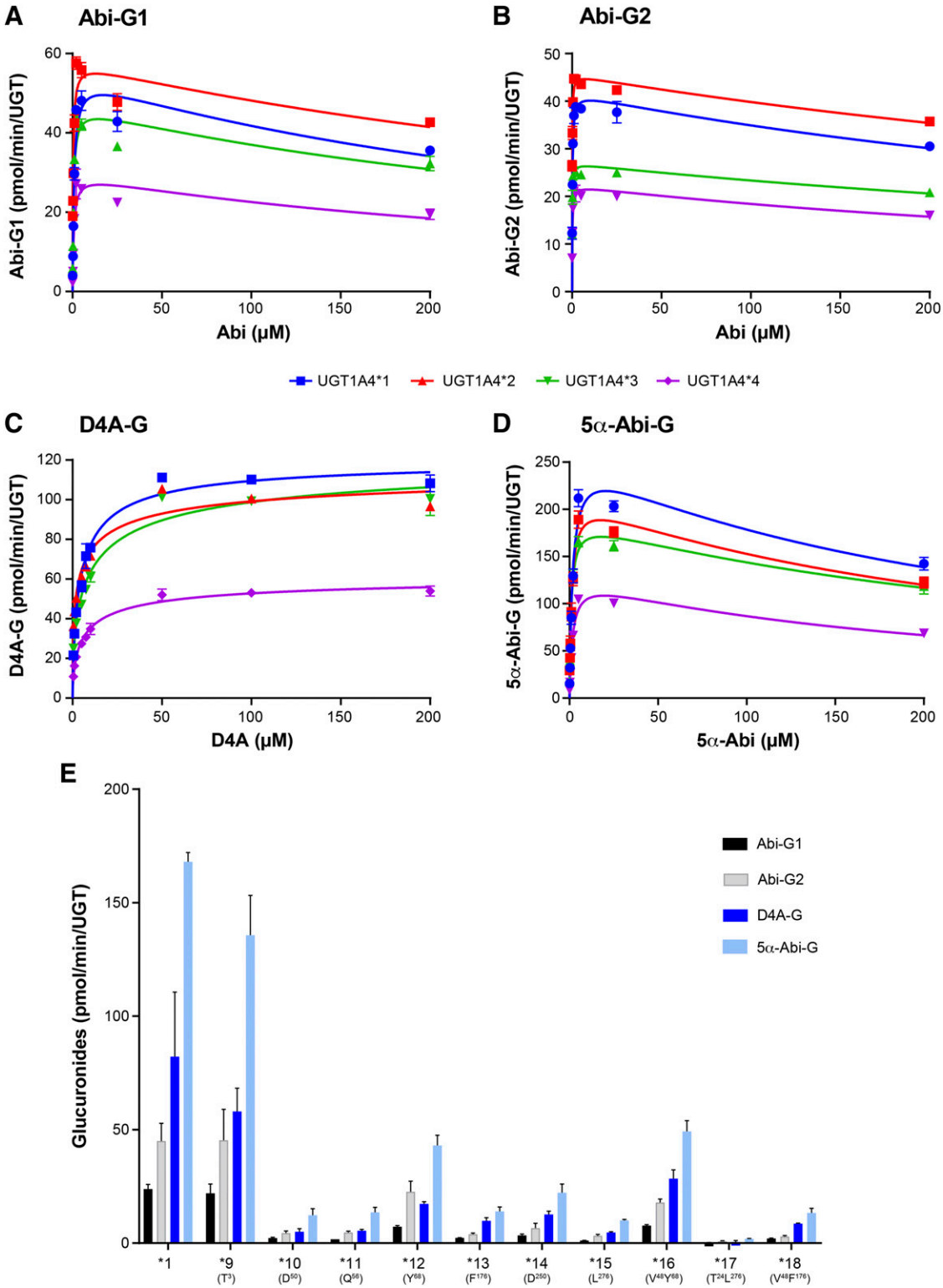

Fig. 5. Formation of Gs of Abi, D4A, and 5α-Abi by UGT1A4 isoenzymes. Kinetic profiles for the formation of Abi (A and B), D4A (C), and 5α-Abi (D) Gs by UGT1A4 common isoenzymes (UGT1A4*1 $R^{11}P^{24}L^{48}$, UGT1A4*2 T^{24}, UGT1A4*3 V^{48}, and UGT1A4*4 W^{11}). UGT1A4 microsomes were incubated with increasing concentrations (up to 200 μM) of substrate for 30 minutes, as described in *Materials and Methods*. Results are expressed as mean ± S.D. of triplicate determinations. (E) Formation of Abi, D4A, and 5α-Abi Gs by additional UGT1A4 isoenzymes for 30 minutes using Abi (2 μM), 5α-Abi (5 μM), and D4A (6 μM). Results are expressed as mean ± S.D. of triplicate determinations of at least two experiments. UGT1A4*1 corresponds to $R^3R^{11}P^{24}L^{48}E^{50}H^{56}H^{68}I^{176}S^{250}I^{276}$. The level of UGT protein assessed by Western blot was used to calculate relative glucuronidation activities.

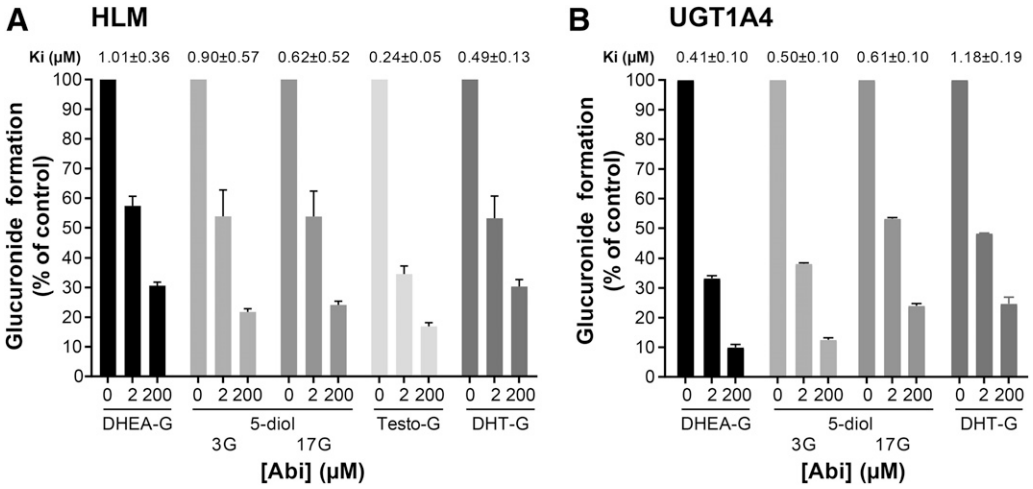

Fig. 6. Dose-dependent inhibition of adrenal precursors (DHEA and A5-diol) and androgens (Testo and DHT) glucuronidation by Abi in HLM expressing a variety of steroid-conjugating UGTs (A) and recombinant UGT1A4 enzyme (B). Activity was measured at constant concentration of substrate (5 μM) with two concentrations of Abi (2 and 200 μM) for 30 minutes, as described in *Materials and Methods*. In the control, no Abi was added. K_i values were derived from an additional set of experiments performed using three different concentrations of substrates and three different concentrations of inhibitor ranging from 0 to 200 μM. Results are expressed as mean ± S.D. of triplicate determinations of at least two experiments. Inhibition models observed were mixed.

UGT1A4*3 had slightly higher affinities. Additional rare variants presented a significantly reduced activity compared with UGT1A4*1 by up to 90% at concentration based on the apparent K_m values, except for UGT1A4*9 (Fig. 5E). This suggests that collectively, these variants UGT1A4 allozymes with coding variations may be associated with reduced hepatic glucuronidation of Abi and its metabolites.

Inhibition of Steroid Glucuronidation by Abi, D4A, 5α-Abi, and Gal. The ability of Abi, its metabolites, and Gal to inhibit glucuronidation of androgens (Testo and DHT) and their adrenal precursors (DHEA and A5-diol) was also evaluated. Conjugation of these steroids is significant in HLM and by the UGT1A4 enzyme, except for Testo, which is a poor substrate of this enzyme. Steroid glucuronidation was inhibited by ≥40% in the presence of 2 μM Abi and reached nearly 90% at 200 μM (Fig. 6). The inhibition pattern by D4A, 5α-Abi, and Gal was similar for HLM and UGT1A4 (Supplemental Fig. 6). This inhibition potency was comparable to the effect of Abi on the hepatic conjugation of tacrolimus, a specific substrate of the UGT1A4 enzyme, whereas no inhibitory effect was observed using 2 μM Abi for bilirubin-G formation performed by the UGT1A1 enzyme in HLM (data not shown). The estimated inhibitory K_i values for these drugs were in the low micromolar range, between 0.17 and 3.59 μM for HLM and UGT1A4 (Supplemental Fig. 8; Table 3). Inhibition was with mixed characteristics according to goodness-of-fit statistics and the Lineweaver–Burk plot graphical representation of experimental data. We observed similar inhibitory effects for Testo-G formation in assays with the androgen-conjugating recombinant UGT2B15 and UGT2B17 enzymes, and the PCa cell line LNCaP, expressing UGT2B15, UGT2B17, and UGT2B28 involved in local androgen inactivation. K_i values observed in the presence of Abi for Testo-G formation were 0.10 ± 0.04, 0.73 ± 0.53, and 3.19 ± 3.74 μM for LNCaP, UGT2B17, and UGT2B15, respectively (Table 3).

Discussion

Our study establishes that Abi, a steroidal CYP17A1 inhibitor, and its downstream active metabolites are conjugated with GlcA in the liver, and that only the UGT1A4 enzyme expressed in human liver is involved. The structurally related androgen receptor axis–targeted agent Gal is also a substrate of the UGT1A4 enzyme. Their glucuronidation in vivo is sustained by the detection of G derivatives of Abi, D4A, and 5α-Abi in plasma samples of PCa patients treated with AA, with a predominance of Abi-G and 5α-Abi-G over D4A-G. We also demonstrate that a number of common and rare UGT1A4 variant allozymes with nonsynonymous substitutions exhibit significantly lower activity for these molecules compared with the reference UGT1A4 enzyme. Based on the results of our in vitro investigations, these pharmacological compounds further emerge as potent inhibitors of their conjugation in the liver by a mixed inhibition model. Abi, D4A, and 5α-Abi also proficiently

TABLE 3

Abi inhibits glucuronidation of adrenal precursors (DHEA and A5-diol) and potent androgens (Testo and DHT)

	Testo-G	DHT-G	DHEA-G	A5-diol-3G	A5-diol-17G
	K_i (μM) for Abi[a]				
HLM	0.24 ± 0.05	0.49 ± 0.13	1.01 ± 0.36	0.90 ± 0.57	0.62 ± 0.52
UGT1A4	n.d.	1.18 ± 0.19	0.41 ± 0.10	0.50 ± 0.10	0.61 ± 0.10
UGT2B15	3.19 ± 3.74	—	—	—	—
UGT2B17	0.73 ± 0.53	—	—	—	—
LNCaP[b]	0.10 ± 0.04	—	—	—	—

L, liver; n.d., not detected because UGT1A4 leads to minor formation of Testo-G; P, prostate; —, not determined.

[a] K_i values were derived from experiments using three concentrations of Abi (5, 25, 200 μM) and three concentrations of Testo, DHT, DHEA, and A5-diol (5, 25, 200 μM). For assays using UGT2B15, UGT2B17, and LNCaP cells, we used lower concentrations of Abi (0.1, 1, 5 μM) and testosterone (1, 5, 25 μM). Results are expressed with mean ± S.D. of triplicate determinations of at least two independent experiments. Inhibition of steroid glucuronidation by D4A and 5α-Abi is presented in Supplemental Fig. 6, and compared with Abi for HLM and UGT1A4. These graphical representations (Fig. 6; Supplemental Fig. 6) only illustrate percentage of inhibition observed in assays using 5 μM androgen in the presence of 0, 2, and 200 μM Abi. Inhibition models observed were mixed.

[b] LNCaP cells are androgen-sensitive human prostate adenocarcinoma cells that express several UGTs, namely UGT2B15, UGT2B17, and UGT2B28.

inhibit steroid glucuronidation catalyzed by UGT1A4 and other UGTs, namely UGT2B15 and UGT2B17, expressed in the liver and PCa cells. This suggests that CYP17A1 inhibitors are conjugated by the glucuronidation pathway, with the potential to affect the UGT-associated drug-metabolizing system and potentially drug-endogenous molecule interactions.

Mass spectral analysis of purified G derivatives from these drugs suggests the formation of O- and N-G products of Abi, and N-G products of D4A and 5α-Abi, but this will require confirmation by NMR. Our work reveals that UGT1A4 catalyzes predominantly their glucuronidation with a potential minor role for UGT1A3. UGT1A4 is a main hepatic drug elimination pathway that participates in the N-glucuronidation of primary, secondary, and aromatic amines, which include many pharmacologically important drugs such as lamotrigine, tamoxifen, and tacrolimus (Argikar and Remmel, 2009; Zhou et al., 2010; Laverdière et al., 2011). UGT1A4 is also capable of conjugating steroidal compounds with hydroxyl groups such as hecogenin (Green and Tephly, 1996), a steroidal saponin aglycone found in the leaves of species from the *Agave* genus and a selective inhibitor of UGT1A4 (Paik et al., 2005). The glucuronidation efficiency of UGT1A4 for several steroids such as 3α-diol (5α-androstane-3α,17β-diol) and pregnanediol (5α-pregnane-3β,20α-diol) was demonstrated with K_m values of 16 and 7.3 μM compared with 18 μM for hecogenin (Green and Tephly, 1996). Zhou et al. (2010) also showed that UGT1A4 displays significant activity for the potent androgen DHT, also revealing the existence of multiple aglycone substrate-binding sites in UGT1A4. In this study, we observed inferior K_m values for Abi and its metabolites in the low-micromolar range varying from 0.61 to 7.4 μM. Based on highly similar kinetic parameters observed for HLM and the UGT1A4 enzyme, we conclude that UGT1A4 is the major UGT contributing to the formation of both N- and O-Gs of Abi, its metabolites, and Gal in vitro. This is also supported by the important loss of activity caused by the selective UGT1A4 inhibitor hecogenin, which hinders drug–G formation by over 50% at low-micromolar concentration (e.g., at K_m value). The extent of the inhibition was comparable for UGT1A4 and liver microsomes, reinforcing the notion that this is likely the primary enzyme involved. Because UGT1A4 is not expressed in the prostate (Ohno and Nakajin, 2009), this reaction would take place primarily in the liver with a minor implication of the intestine. UGT1A3 is potentially responsible for the low activity observed in the human intestine microsomes based on its weak activity and its expression in this tissue (Ohno and Nakajin, 2009; Margaillan et al., 2015). Moreover, the lack of inhibition for UGT1A1-mediated bilirubin conjugation is also consistent with the low occurrence of hyperbilirubinemia observed in clinical trials (Fizazi et al., 2012, 2019; Smith et al., 2017). Besides, the microsomal assays exhibited complex glucuronidation kinetics, including substrate inhibition. Previous report showed that UGTs exhibit atypical kinetics in vitro, potentially explained by existence of two binding sites or substrate-induced changes in enzyme conformation (Kaivosaari et al., 2008; Uchaipichat et al., 2008; Zhou et al., 2010).

UGT1A4 displays significant variability in its coding sequence with three common reported allozymes, UGT1A4*2, UGT1A4*3, and UGT1A4*4, presenting frequencies of 1.8%, 13.8%, and 1.4%, respectively, according to 1000 genomes. These variants have been functionally characterized for different drugs in vitro and in vivo (Mori et al., 2005; Benoit-Biancamano et al., 2009a; Erickson-Ridout et al., 2011; Laverdière et al., 2011; Zhou et al., 2011; Edavana et al., 2013; Reimers et al., 2016; Sutiman et al., 2016; Smith et al., 2018). These variant allozymes displayed kinetic parameters comparable to those of the reference UGT1A4*1 enzyme, except UGT1A4*4, which had a significantly lower velocity for Abi and its metabolites, consistent with the reported impact of this specific variant on tamoxifen (Benoit-Biancamano et al., 2009a; Zhou et al., 2011). We also explored the impact of additional rare polymorphisms with frequencies below 1% that all presented much inferior activities, suggesting that collectively these UGT1A4 variant isoforms could potentially impact the hepatic glucuronidation of Abi and its metabolites. The impact of these UGT1A4 germline variants on the overall hepatic metabolism, response, and hepatic toxicity will require additional studies.

The data reported in this work also provide insights into the potential inhibitory effect of Abi and its active metabolites on steroid glucuronidation. These observations are in line with the reported inhibitory activity of Abi and Gal on the sulfonation of DHEA (Yip et al., 2018). Abi, D4A, 5α-Abi, and Gal exhibited strong inhibition toward glucuronidation of adrenal precursors (DHEA and A5-diol) and potent androgens (Testo and DHT) with comparable inhibitory profiles. The apparent K_i values (<10 μM for Testo-G formation) were in order of magnitude similar to the plasma drug concentrations achieved in PCa patients (Alyamani et al., 2018). In comparison, the antiandrogen finasteride was shown to inhibit UGT1A4-mediated activity using trifluoperazine as a substrate with a K_i of 6.05 μM (Lee et al., 2015). Our results further suggest that Abi and its metabolites not only inhibit hepatic glucuronidation of androgens but also glucuronidation of androgens by UGT2B15 and UGT2B17 enzymes highly expressed in the prostate (Chouinard et al., 2004). This is reinforced by the inhibition of androgen glucuronidation in LNCaP cells that express UGT2B15, UGT2B17, and other UGTs. The inhibition potential R (R value = 1 + [I]/Ki) was calculated to estimate the potential of Abi to block androgen metabolism by UGTs, as previously done (Deb et al., 2014; Oda et al., 2015), using the peak plasma concentration (I) of 2.2 μM (Ryan et al., 2010), and K_i values from liver microsomes (K_i = 0.24–1.01 μM for Testo, DHT, DHEA, and A5-diol) and prostate cells (K_i = 0.10 μM for Testo). R values of Abi were all above the cutoff R value >1.1 for having the potential to cause drug–drug interactions in vivo (Yu et al., 2017). R values ranged from 3.2 to 23.0, suggesting that the levels of Abi attained in humans could potentially inhibit the catabolism of androgens in vivo. However, as the metabolism of Abi is complex and involves multiple steroid-biotransforming enzymes, also expressed locally in PCa cells, additional in vivo evidence is needed. Although Abi leads to a major depletion of circulating steroid hormones, it is tempting to speculate that this inhibitory impact on steroid inactivation pathways may potentially alter pre-receptor control of androgen metabolism in patients with incomplete suppression of adrenal androgens. It may also be relevant when PCa cells become Abi-resistant, where the glucuronidation inhibition of Testo and DHT might impact PCa growth.

In conclusion, we have demonstrated that the metabolism of CYP17A1 steroidal inhibitors continues downstream to the final glucuronidation steps as observed for steroid biotransformation pathways. We showed that the hepatic UGT1A4 enzyme is the primary enzyme involved in this conjugation process and that coding polymorphisms affecting this gene significantly reduced conjugation capacity in vitro. Additional translational pharmacogenomics studies are required to establish the potential clinical relevance of the UGT1A4 pathway to drug metabolism and clinical response.

Acknowledgments

We are thankful to all participating patients and clinical staff who have made this scientific contribution possible.

Authorship Contributions

Participated in research design: Lévesque, Guillemette.
Conducted experiments: Vaillancourt, Turcotte, Caron, Villeneuve.
Contributed new reagents or analytic tools: Turcotte, Caron.

Performed data analysis: Vaillancourt, Turcotte, Caron, Villeneuve, Guillemette.

Wrote or contributed to the writing of the manuscript: Vaillancourt, Turcotte, Caron, Villeneuve, Lacombe, Pouliot, Lévesque, Guillemette.

References

Alyamani M, Emamekhoo H, Park S, Taylor J, Almassi N, Upadhyay S, Tyler A, Berk MP, Hu B, Hwang TH, et al. (2018) HSD3B1(1245A>C) variant regulates dueling abiraterone metabolite effects in prostate cancer. *J Clin Invest* **128**:3333–3340.

Alyamani M, Li Z, Berk M, Li J, Tang J, Upadhyay S, Auchus RJ, and Sharifi N (2017) Steroidogenic metabolism of galeterone reveals a diversity of biochemical activities. *Cell Chem Biol* **24**:825–832.e6.

Argikar UA and Remmel RP (2009) Variation in glucuronidation of lamotrigine in human liver microsomes. *Xenobiotica* **39**:355–363.

Beaulieu M, Lévesque E, Hum DW, and Bélanger A (1996) Isolation and characterization of a novel cDNA encoding a human UDP-glucuronosyltransferase active on C19 steroids. *J Biol Chem* **271**:22855–22862.

Beer TM, Armstrong AJ, Rathkopf DE, Loriot Y, Sternberg CN, Higano CS, Iversen P, Bhattacharya S, Carles J, Chowdhury S, et al.; PREVAIL Investigators (2014) Enzalutamide in metastatic prostate cancer before chemotherapy. *N Engl J Med* **371**:424–433.

Benoit-Biancamano MO, Adam JP, Bernard O, Court MH, Leblanc MH, Caron P, and Guillemette C (2009a) A pharmacogenetics study of the human glucuronosyltransferase UGT1A4. *Pharmacogenet Genomics* **19**:945–954.

Benoit-Biancamano MO, Connelly J, Villeneuve L, Caron P, and Guillemette C (2009b) Deferiprone glucuronidation by human tissues and recombinant UDP glucuronosyltransferase 1A6: an in vitro investigation of genetic and splice variants. *Drug Metab Dispos* **37**:322–329.

Bouhajib M and Tayab Z (2019) Evaluation of the pharmacokinetics of abiraterone acetate and abiraterone following single-dose administration of abiraterone acetate to healthy subjects. *Clin Drug Investig* **39**:309–317.

Caron P, Turcotte V, Lévesque E, and Guillemette C (2019) An LC-MS/MS method for quantification of abiraterone, its active metabolites D(4)-abiraterone (D4A) and 5α-abiraterone, and their inactive glucuronide derivatives. *J Chromatogr B Analyt Technol Biomed Life Sci* **1104**: 249–255.

Chouinard S, Pelletier G, Bélanger A, and Barbier O (2004) Cellular specific expression of the androgen-conjugating enzymes UGT2B15 and UGT2B17 in the human prostate epithelium. *Endocr Res* **30**:717–725.

Deb S, Chin MY, Adomat H, and Guns ES (2014) Abiraterone inhibits 1α,25-dihydroxyvitamin D3 metabolism by CYP3A4 in human liver and intestine in vitro. *J Steroid Biochem Mol Biol* **144**:50–58.

Edavana VK, Dhakal IB, Williams S, Penney R, Boysen G, Yao-Borengasser A, and Kadlubar S (2013) Potential role of UGT1A4 promoter SNPs in anastrozole pharmacogenomics. *Drug Metab Dispos* **41**:870–877.

Erickson-Ridout KK, Zhu J, and Lazarus P (2011) Olanzapine metabolism and the significance of UGT1A448V and UGT2B1067Y variants. *Pharmacogenet Genomics* **21**:539–551.

Fizazi K, Scher HI, Molina A, Logothetis CJ, Chi KN, Jones RJ, Staffurth JN, North S, Vogelzang NJ, Saad F, et al.; COU-AA-301 Investigators (2012) Abiraterone acetate for treatment of metastatic castration-resistant prostate cancer: final overall survival analysis of the COU-AA-301 randomised, double-blind, placebo-controlled phase 3 study. *Lancet Oncol* **13**:983–992.

Fizazi K, Tran N, Fein L, Matsubara N, Rodriguez-Antolin A, Alekseev BY, Özgüroğlu M, Ye D, Feyerabend S, Protheroe A, et al. (2019) Abiraterone acetate plus prednisone in patients with newly diagnosed high-risk metastatic castration-sensitive prostate cancer (LATITUDE): final overall survival analysis of a randomised, double-blind, phase 3 trial. *Lancet Oncol* **20**:686–700.

Green MD and Tephly TR (1996) Glucuronidation of amines and hydroxylated xenobiotics and endobiotics catalyzed by expressed human UGT1.4 protein. *Drug Metab Dispos* **24**:356–363.

Guillemette C, Lévesque É, and Rouleau M (2014) Pharmacogenomics of human uridine diphospho-glucuronosyltransferases and clinical implications. *Clin Pharmacol Ther* **96**:324–339.

Hu DG, Meech R, McKinnon RA, and Mackenzie PI (2014) Transcriptional regulation of human UDP-glucuronosyltransferase genes. *Drug Metab Rev* **46**:421–458.

Kaivosaari S, Toivonen P, Aitio O, Sipilä J, Koskinen M, Salonen JS, and Finel M (2008) Regio- and stereospecific N-glucuronidation of medetomidine: the differences between UDP glucuronosyltransferase (UGT) 1A4 and UGT2B10 account for the complex kinetics of human liver microsomes. *Drug Metab Dispos* **36**:1529–1537.

Laverdière I, Caron P, Harvey M, Lévesque É, and Guillemette C (2011) In vitro investigation of human UDP-glucuronosyltransferase isoforms responsible for tacrolimus glucuronidation: predominant contribution of UGT1A4. *Drug Metab Dispos* **39**:1127–1130.

Lee SJ, Park JB, Kim D, Bae SH, Chin YW, Oh E, and Bae SK (2015) In vitro selective inhibition of human UDP-glucuronosyltransferase (UGT) 1A4 by finasteride, and prediction of in vivo drug-drug interactions. *Toxicol Lett* **232**:458–465.

Lévesque E, Girard H, Journault K, Lépine J, and Guillemette C (2007) Regulation of the UGT1A1 bilirubin-conjugating pathway: role of a new splicing event at the UGT1A locus. *Hepatology* **45**:128–138.

Li Z, Alyamani M, Li J, Rogacki K, Abazeed M, Upadhyay SK, Balk SP, Taplin ME, Auchus RJ, and Sharifi N (2016) Redirecting abiraterone metabolism to fine-tune prostate cancer antiandrogen therapy. *Nature* **533**:547–551.

Li Z, Bishop AC, Alyamani M, Garcia JA, Dreicer R, Bunch D, Liu J, Upadhyay SK, Auchus RJ, and Sharifi N (2015) Conversion of abiraterone to D4A drives anti-tumour activity in prostate cancer. *Nature* **523**:347–351.

Margaillan G, Rouleau M, Klein K, Fallon JK, Caron P, Villeneuve L, Smith PC, Zanger UM, and Guillemette C (2015) Multiplexed targeted quantitative proteomics predicts hepatic glucuronidation potential. *Drug Metab Dispos* **43**:1331–1335.

Miller KD, Siegel RL, Lin CC, Mariotto AB, Kramer JL, Rowland JH, Stein KD, Alteri R, and Jemal A (2016) Cancer treatment and survivorship statistics, 2016. *CA Cancer J Clin* **66**:271–289.

Montgomery RB, Mostaghel EA, Vessella R, Hess DL, Kalhorn TF, Higano CS, True LD, and Nelson PS (2008) Maintenance of intratumoral androgens in metastatic prostate cancer: a mechanism for castration-resistant tumor growth. *Cancer Res* **68**:4447–4454.

Mori A, Maruo Y, Iwai M, Sato H, and Takeuchi Y (2005) UDP-glucuronosyltransferase 1A4 polymorphisms in a Japanese population and kinetics of clozapine glucuronidation. *Drug Metab Dispos* **33**:672–675.

Oda S, Fujiwara R, Kutsuno Y, Fukami T, Itoh T, Yokoi T, and Nakajima M (2015) Targeted screen for human UDP-glucuronosyltransferases inhibitors and the evaluation of potential drug-drug interactions with zafirlukast. *Drug Metab Dispos* **43**:812–818.

Ohno S and Nakajin S (2009) Determination of mRNA expression of human UDP-glucuronosyltransferases and application for localization in various human tissues by real-time reverse transcriptase-polymerase chain reaction. *Drug Metab Dispos* **37**:32–40.

Paik SY, Koh KH, Beak SM, Paek SH, and Kim JA (2005) The essential oils from Zanthoxylum schinifolium pericarp induce apoptosis of HepG2 human hepatoma cells through increased production of reactive oxygen species. *Biol Pharm Bull* **28**:802–807.

Reimers A, Sjursen W, Helde G, and Brodtkorb E (2016) Frequencies of UGT1A4*2 (P24T) and *3 (L48V) and their effects on serum concentrations of lamotrigine. *Eur J Drug Metab Pharmacokinet* **41**:149–155.

Ryan CJ, Smith MR, Fizazi K, Saad F, Mulders PF, Sternberg CN, Miller K, Logothetis CJ, Shore ND, Small EJ, et al.; COU-AA-302 Investigators (2015) Abiraterone acetate plus prednisone versus placebo plus prednisone in chemotherapy-naive men with metastatic castration-resistant prostate cancer (COU-AA-302): final overall survival analysis of a randomised, double-blind, placebo-controlled phase 3 study. *Lancet Oncol* **16**:152–160.

Ryan CJ, Smith MR, Fong L, Rosenberg JE, Kantoff P, Raynaud F, Martins V, Lee G, Kheoh T, Kim J, et al. (2010) Phase I clinical trial of the CYP17 inhibitor abiraterone acetate demonstrating clinical activity in patients with castration-resistant prostate cancer who received prior ketoconazole therapy. *J Clin Oncol* **28**:1481–1488.

Scher HI, Fizazi K, Saad F, Taplin ME, Sternberg CN, Miller K, de Wit R, Mulders P, Chi KN, Shore ND, et al.; AFFIRM Investigators (2012) Increased survival with enzalutamide in prostate cancer after chemotherapy. *N Engl J Med* **367**:1187–1197.

Smith MR, Saad F, Rathkopf DE, Mulders PFA, de Bono JS, Small EJ, Shore ND, Fizazi K, Kheoh T, Li J, et al. (2017) Clinical outcomes from androgen signaling-directed therapy after treatment with abiraterone acetate and prednisone in patients with metastatic castration-resistant prostate cancer: post hoc analysis of COU-AA-302. *Eur Urol* **72**:10–13.

Smith RL, Haslemo T, Chan HF, Refsum H, and Molden E (2018) Clinically relevant effect of UGT1A4*3 on lamotrigine serum concentration is restricted to postmenopausal women - a study matching therapeutic drug monitoring and genotype data from 534 patients. *Ther Drug Monit* **40**: 567–571.

Sutiman N, Lim JSL, Muerdter TE, Singh O, Cheung YB, Ng RCH, Yap YS, Wong NS, Ang PCS, Dent R, et al. (2016) Pharmacogenetics of UGT1A4, UGT2B7 and UGT2B15 and their influence on tamoxifen disposition in Asian breast cancer patients. *Clin Pharmacokinet* **55**:1239–1250.

Tucci M, Scagliotti GV, and Vignani F (2015) Metastatic castration-resistant prostate cancer: time for innovation. *Future Oncol* **11**:91–106.

Uchaipichat V, Galetin A, Houston JB, Mackenzie PI, Williams JA, and Miners JO (2008) Kinetic modeling of the interactions between 4-methylumbelliferone, 1-naphthol, and zidovudine glucuronidation by udp-glucuronosyltransferase 2B7 (UGT2B7) provides evidence for multiple substrate binding and effector sites. *Mol Pharmacol* **74**:1152–1162.

Villeneuve L, Girard H, Fortier LC, Gagné JF, and Guillemette C (2003) Novel functional polymorphisms in the UGT1A7 and UGT1A9 glucuronidating enzymes in Caucasian and African-American subjects and their impact on the metabolism of 7-ethyl-10-hydroxycamptothecin and flavopiridol anticancer drugs. *J Pharmacol Exp Ther* **307**:117–128.

Yip CKY, Bansal S, Wong SY, and Lau AJ (2018) Identification of galeterone and abiraterone as inhibitors of dehydroepiandrosterone sulfonation catalyzed by human hepatic cytosol, SULT2A1, SULT2B1b, and SULT1E1. *Drug Metab Dispos* **46**:470–482.

Yu J, Zhou Z, Owens KH, Ritchie TK, and Ragueneau-Majlessi I (2017) What can be learned from recent new drug applications? A systematic review of drug interaction data for drugs approved by the US FDA in 2015. *Drug Metab Dispos* **45**:86–108.

Zhou J, Argikar UA, and Remmel RP (2011) Functional analysis of UGT1A4(P24T) and UGT1A4(L48V) variant enzymes. *Pharmacogenomics* **12**:1671–1679.

Zhou J, Tracy TS, and Remmel RP (2010) Glucuronidation of dihydrotestosterone and transandrosterone by recombinant UDP-glucuronosyltransferase (UGT) 1A4: evidence for multiple UGT1A4 aglycone binding sites. *Drug Metab Dispos* **38**:431–440.

Address correspondence to: Dr. Chantal Guillemette, Pharmacogenomics Laboratory, CHU de Québec Research Center, 2705 Boulevard Laurier, R4701.5, Québec, Canada G1V 4G2. E-mail: Chantal.Guillemette@crchudequebec.ulaval.ca

Glucuronidation of Abiraterone and its Pharmacologically Active Metabolites by UGT1A4, Influence of Polymorphic Variants and their Potential as Inhibitors of Steroids Glucuronidation.

Joanie Vaillancourt, Véronique Turcotte, Patrick Caron, Lyne Villeneuve, Louis Lacombe, Frédéric Pouliot, Éric Lévesque, Chantal Guillemette

Supplemental tables and figures

Supplementary Table 1 Enzyme kinetics of Abi, D4A and 5α-Abi glucuronidation by UGT1A4 alloenzymes

UGT1A4 alloenzyme	Apparent K_m (μM)		Relative V_{max} (pmol/min/mg protein)		Clearance (μl/min/mg)	
			Abi-G1			
UGT1A4*1	0.79 ± 0.05		43.13 ± 10.76		54.22 ± 11.38	
UGT1A4*2	0.22 ± 0.14	**	54.68 ± 4.25		307.20 ± 182.23	
UGT1A4*3	0.52 ± 0.00	***	42.10 ± 6.42		80.59 ± 11.63	
UGT1A4*4	0.71 ± 0.10		23.18 ± 5.96	*	33.49 ± 10.39	
			Abi-G2			
UGT1A4*1	0.20 ± 0.02		45.82 ± 7.91		231.40 ± 58.71	
UGT1A4*2	0.07 ± 0.01	***	47.77 ± 3.14		720.23 ± 161.71	*
UGT1A4*3	0.11 ± 0.02	*	26.01 ± 1.33		235.96 ± 62.64	
UGT1A4*4	0.18 ± 0.02		23.58 ± 4.24	*	133.48 ± 7.69	
			D4A-G			
UGT1A4*1	5.22 ± 0.78		112.28 ± 12.92		21.92 ± 5.75	
UGT1A4*2	4.87 ± 1.81		118.38 ± 1.45		26.15 ± 10.00	
UGT1A4*3	9.30 ± 1.31		120.49 ± 10.37		13.00 ± 0.71	
UGT1A4*4	5.80 ± 1.35		58.14 ± 6.80	*	10.17 ± 1.20	
			5α-Abi-G			
UGT1A4*1	1.85 ± 0.15		213.12 ± 40.09		116.49 ± 28.16	
UGT1A4*2	1.12 ± 0.12	**	179.04 ± 49.97		158.62 ± 27.98	
UGT1A4*3	0.99 ± 0.00	**	178.33 ± 16.27		179.30 ± 15.95	
UGT1A4*4	1.44 ± 0.27		107.86 ± 17.88	*	75.26 ± 1.58	

Results are expressed with Mean ± S.D. of triplicate determinations of at least two independent experiments. Relative V_{max} values were adjusted for UGT1A4 protein content assessed by western blotting (Laverdiere et al., 2011). UGT1A4*1 ($R^{11}P^{24}L^{48}$), UGT1A4*2 (T^{24}), UGT1A4*3 (V^{48}), UGT1A4*4 (W^{11}) * $P < 0.05$; ** $P < 0.01$; *** $P < 0.005$. SD: standard deviation; G: glucuronide.

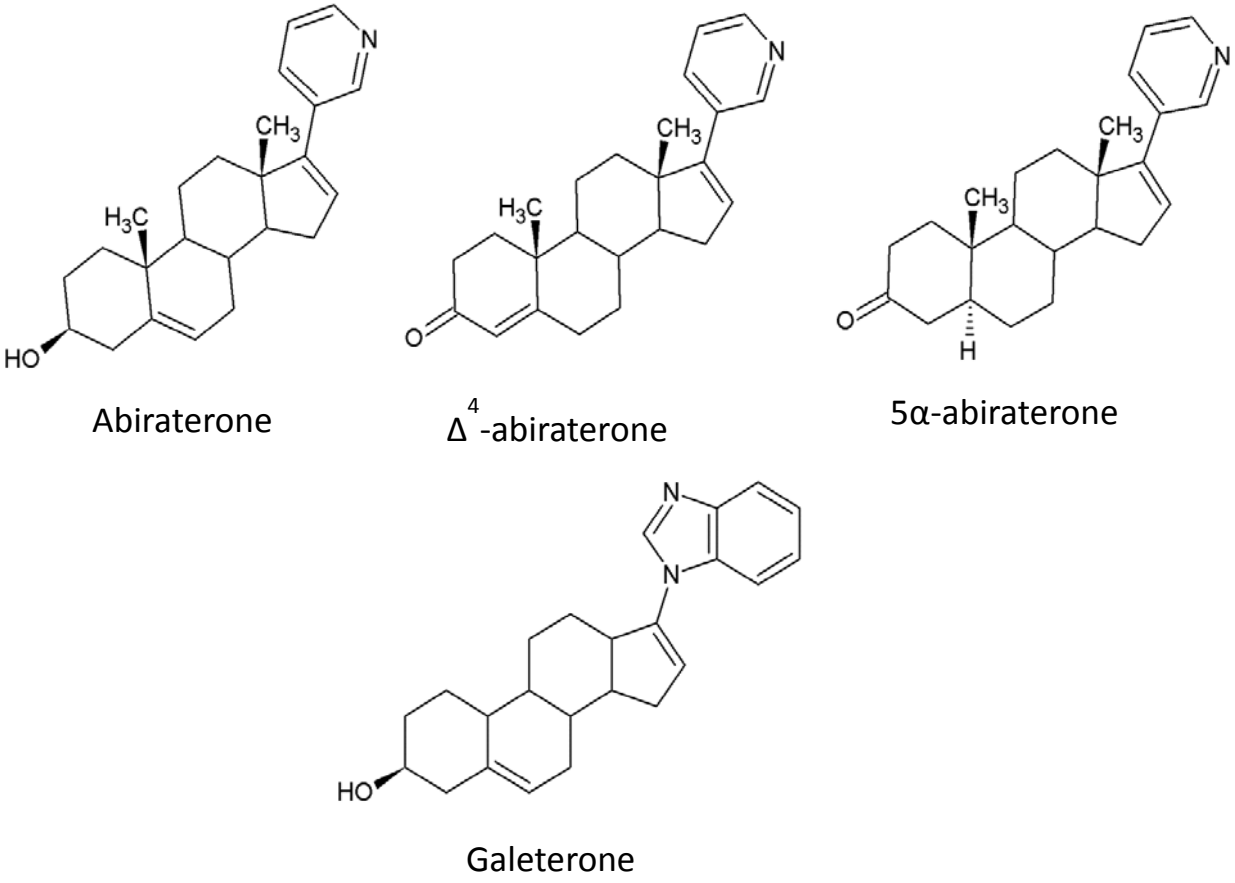

Supplementary Figure 1. Structures of compounds relevant to this study.

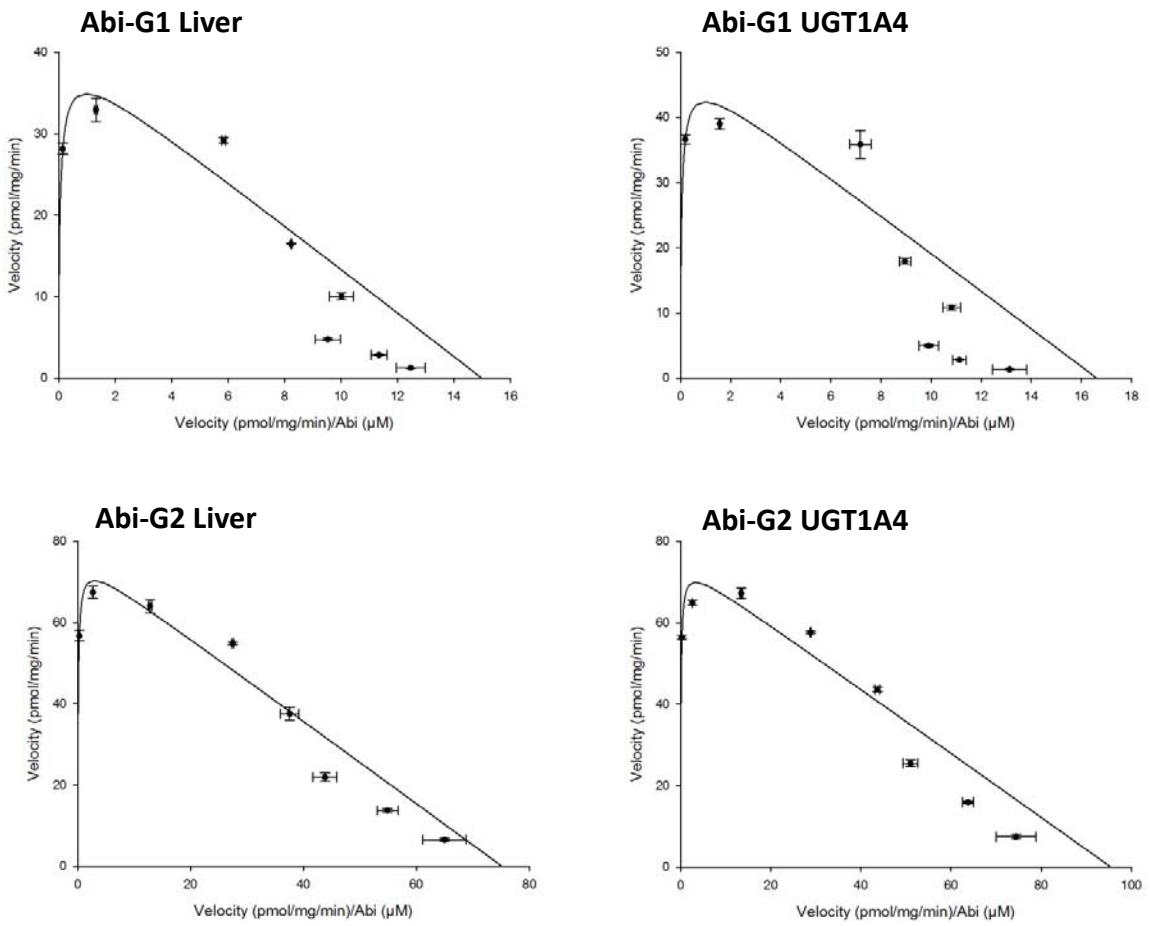

Supplementary Figure 2. Eadie-Hofstee regressions for the formation of glucuronides of Abi by human liver microsomes (HLM) and recombinant UGT1A4 enzyme. HLM and UGT1A4 were incubated in the presence of concentrations ranging from 0 to 200 µM of Abi for 30 min as described in Materials and Methods. Results are expressed as mean ± S.D. of triplicate determinations of one representative experiment. S.D.: standard deviation; G: glucuronide.

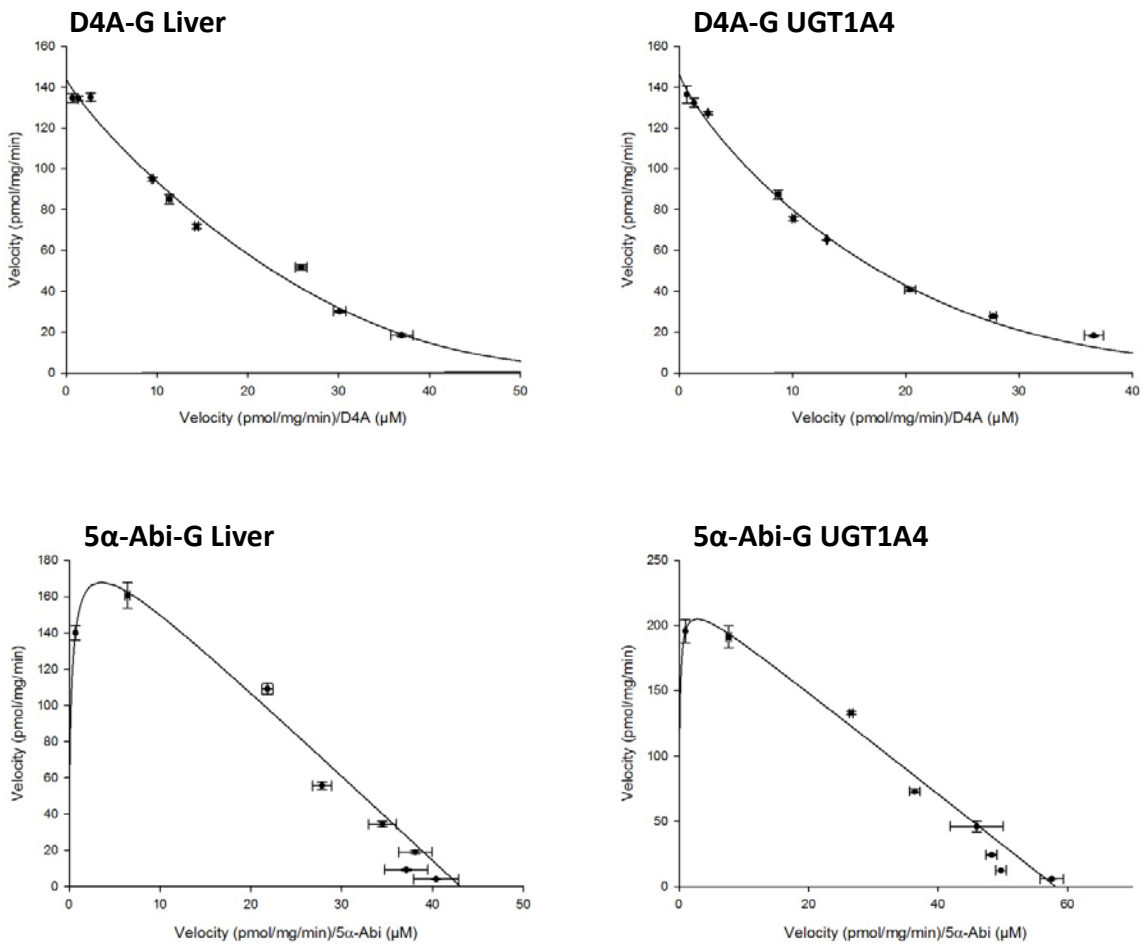

Supplementary Figure 3. Eadie-Hofstee regressions for the formation of glucuronides of D4A and 5α-Abi by human liver microsomes (HLM) and recombinant UGT1A4 enzyme. HLM and UGT1A4 were incubated in the presence of concentrations ranging from 0 to 200 μM of D4A or 5α-Abi for 30 min as described in Materials and Methods. Results are expressed as mean ± S.D. of triplicate determinations of one representative experiment. S.D.: standard deviation; G: glucuronide.

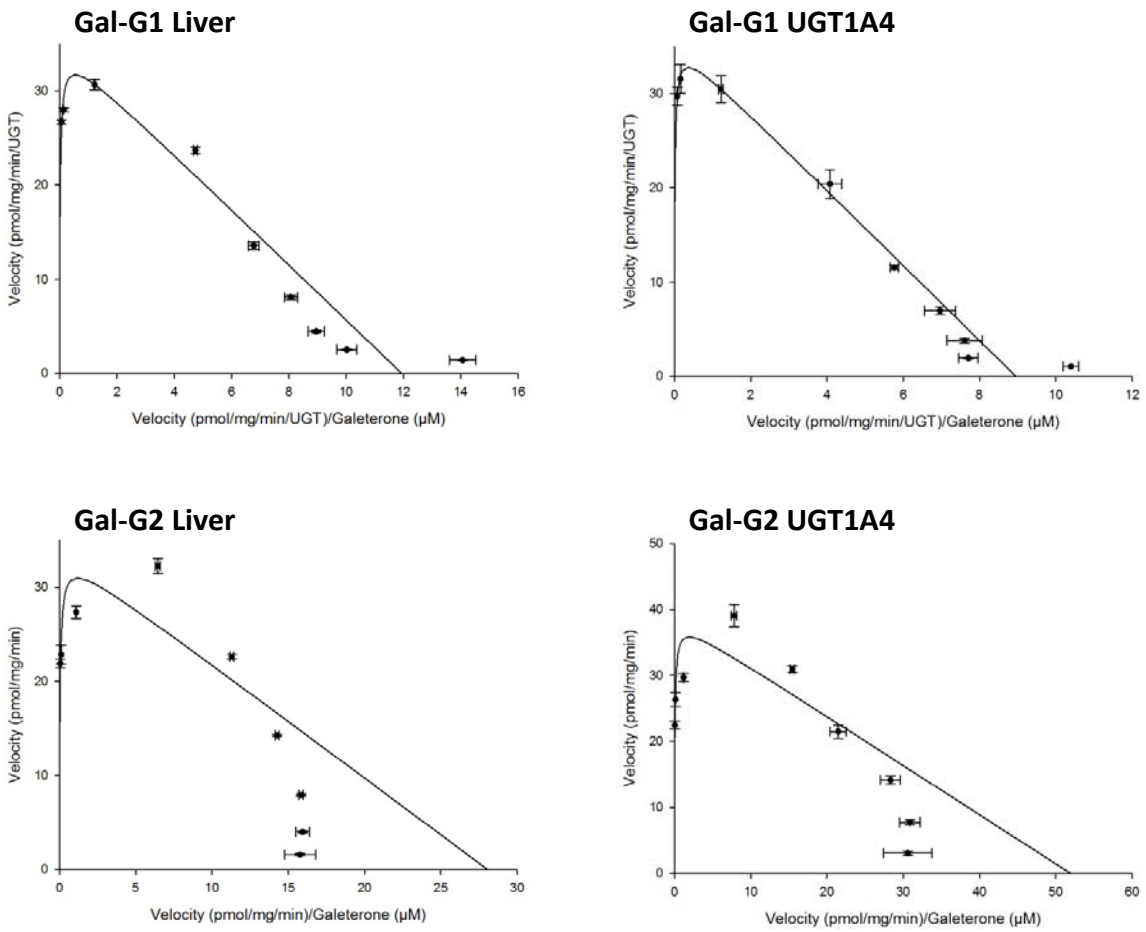

Supplementary Figure 4. Eadie-Hofstee regressions for the formation of glucuronides of Gal by human liver microsomes (HLM) and recombinant UGT1A4 enzyme. HLM and UGT1A4 were incubated in the presence of concentrations ranging from 0 to 400 μM of Gal for 30 min as described in Materials and Methods. Results are expressed as mean ± S.D. of triplicate determinations of one representative experiment. S.D.: standard deviation; G: glucuronide.

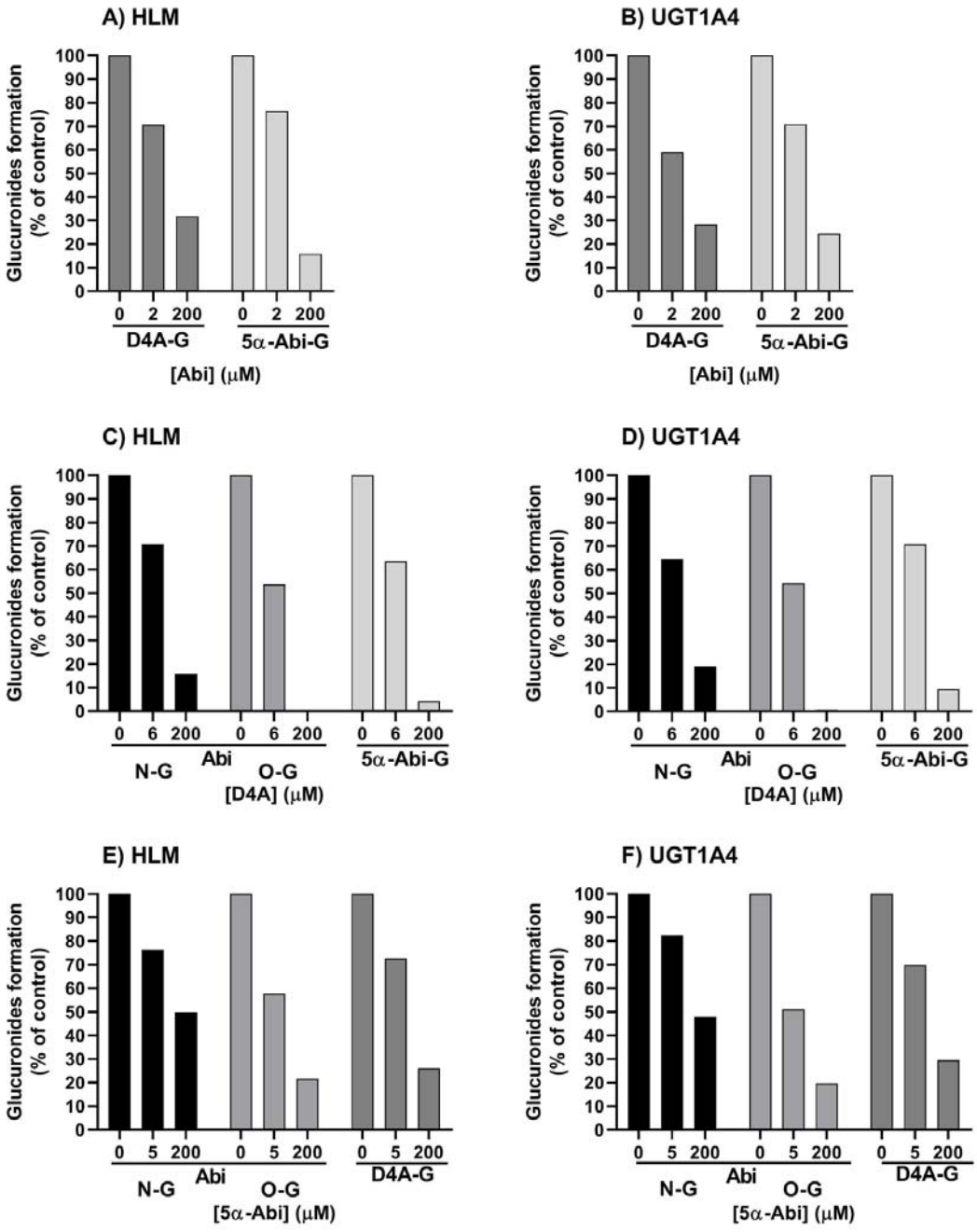

Supplementary Figure 5. Dose-dependent inhibition of drug glucuronide formation by Abi, D4A, 5α-Abi in human liver microsomes (HLM) (A, C, E) and recombinant UGT1A4 enzyme (B, D, F). Activity was measured at a constant concentration of substrate at K_m concentrations (Abi (2 μM), 5α-Abi (5 μM), and D4A (6 μM)) with different concentrations of inhibitor (0, K_m concentrations and 200 μM) for 30 min as described in Materials and Methods. Results are expressed as mean ± S.D. of triplicate determinations of at least two experiments. S.D.: standard deviation; G: glucuronide.

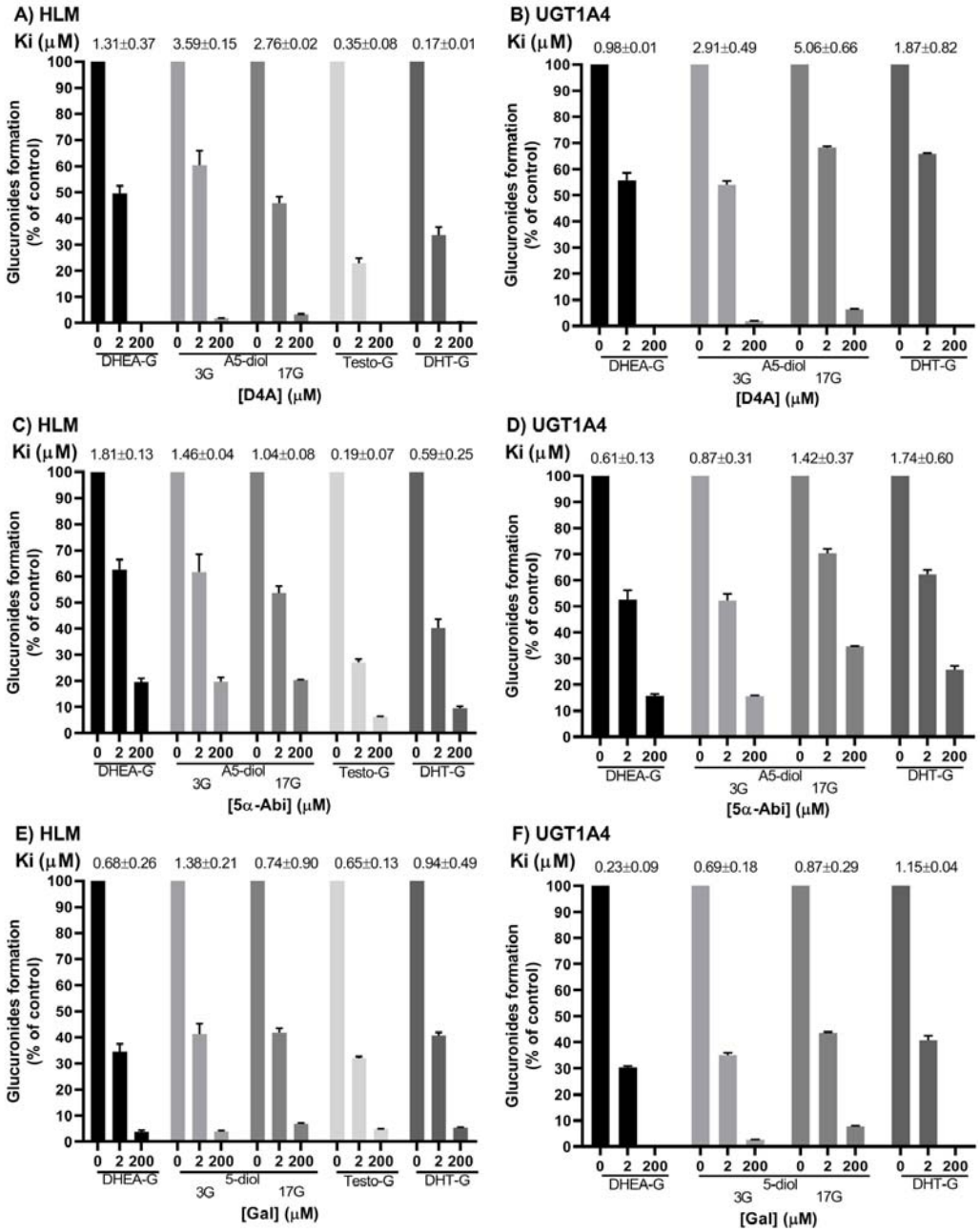

Supplementary Figure 6. Dose-dependent inhibition of glucuronidation of adrenal precursors (DHEA and A5-diol) and androgens (Testo and DHT) by D4A, 5α-Abi and Gal in human liver microsomes (HLM) (A, C, E) and recombinant UGT1A4 enzyme (B, D, F). Activity was measured at a constant concentration of substrate (5 μM) with different concentrations of inhibitor (0, 2 and 200 μM) for 30 min as described in Materials and Methods. K_i values were derived from experiments performed using three concentrations of Abi (5, 25, 200 μM) and three concentrations of Testo, DHT, DHEA and A5-diol (5, 25, 200 μM). For assays using UGT2B15, UGT2B17 and LNcaP cells, we used lower concentrations of Abi (0.1, 1, 5 μM) and testosterone (1, 5, 25 μM). Results are expressed as mean ± S.D. of triplicate determinations of at least two experiments. S.D.: standard deviation; G: glucuronide.

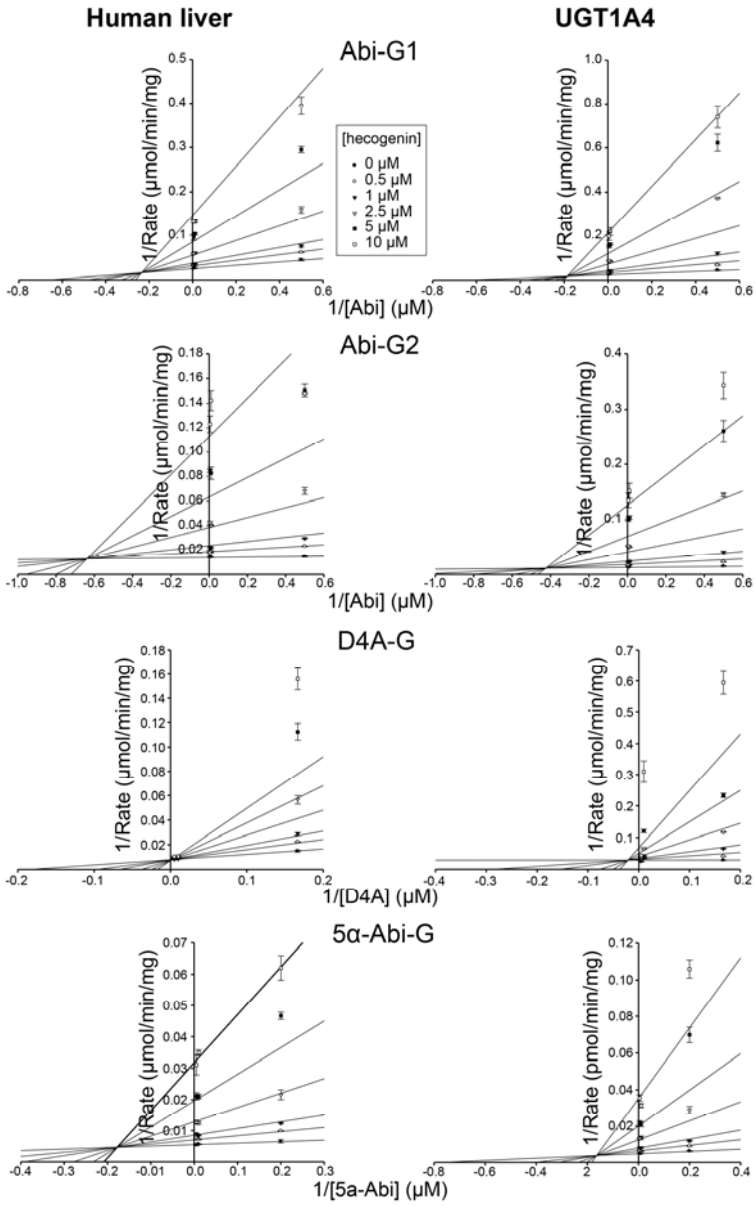

Supplementary Figure 7. Lineweaver-Burk plots for inhibition of drug glucuronidation by hecogenin in human liver microsomes (HLM) (left) and recombinant UGT1A4 enzyme (right). K_i values were derived from experiments performed using the following concentrations of hecogenin (0.5, 1, 2.5, 5, 10 µM) and three different concentrations of each substrate (Abi: 2, 100, 200 µM; D4A 6, 100, 200 µM; 5α-Abi: 5, 100, 200 µM; Gal: 0.5, 2 and 5 µM). Results are expressed as mean ± S.D. of triplicate determinations of at least two experiments. S.D.: standard deviation; G: glucuronide.

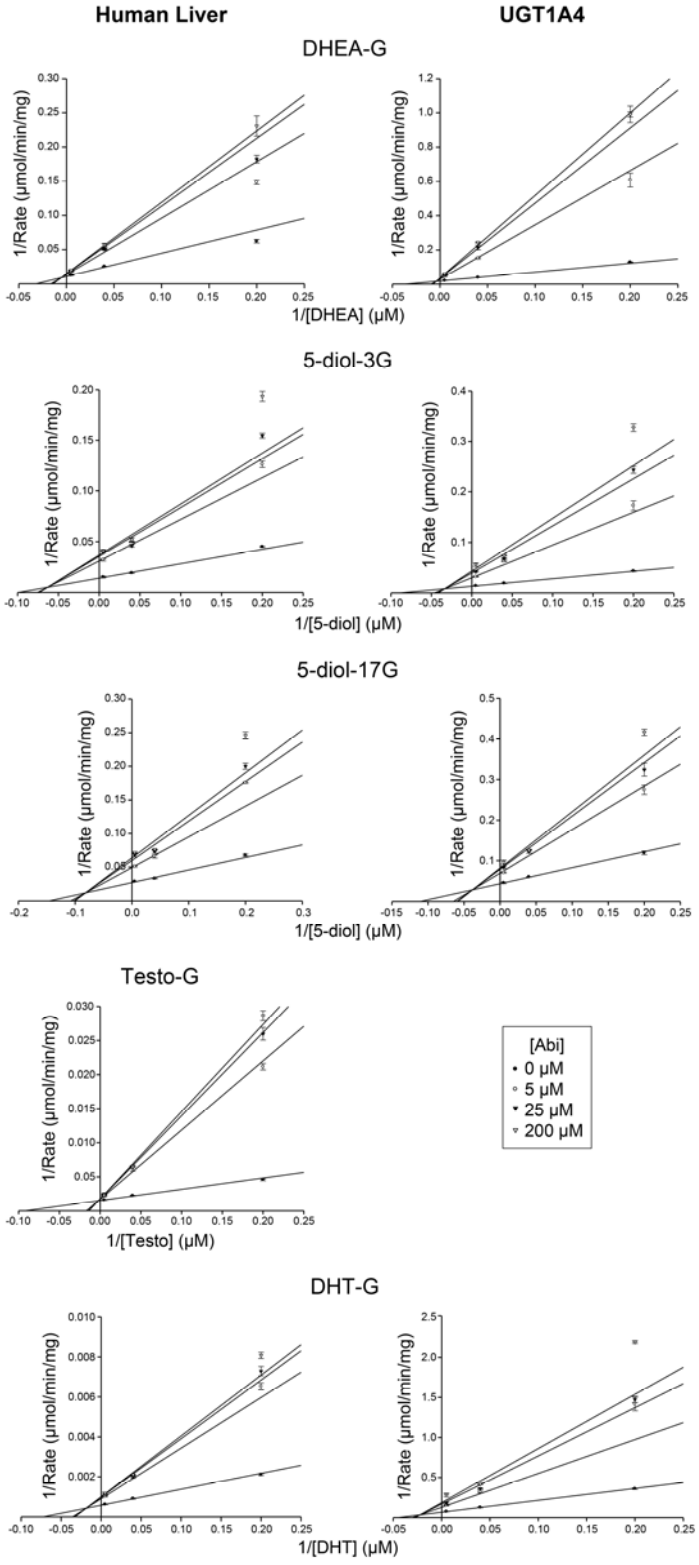

Supplementary Figure 8. Lineweaver-Burk plots for inhibition of glucuronidation of adrenal precursors (DHEA and A5-diol) and androgens (Testo and DHT) by Abi in human liver microsomes (HLM) (right) and recombinant UGT1A4 enzyme (left). K_i values were derived from experiments performed using three concentrations of Abi (5, 25, 200 µM) and three concentrations of Testo, DHT, DHEA and A5-diol (5, 25, 200 µM). Results are expressed as mean ± S.D. of triplicate determinations of at least two experiments. S.D.: standard deviation; G: glucuronide.